Efficacy and Mode of Action of a Direct Inhibitor of Mycobacterium abscessus InhA

Matthéo Alcaraz, Françoise Roquet-Banères, Stephen Adonai Leon-Icaza, Jan Abendroth, Yves-Marie Boudehen, Céline Cougoule, Thomas E Edwards, Laurent Kremer

Efficacy and mode of action of a direct inhibitor of *Mycobacterium abscessus* InhA

Matthéo Alcaraz[1], Françoise Roquet-Banères[1], Stephen Adonai Leon-Icaza[3], Jan Abendroth[4,5], Yves-Marie Boudehen[1], Céline Cougoule[3], Thomas E. Edwards[4,5], and Laurent Kremer[1,2,#]

[1]Centre National de la Recherche Scientifique UMR 9004, Institut de Recherche en Infectiologie de Montpellier (IRIM), Université de Montpellier, 1919 route de Mende, 34293, Montpellier, France.

[2]INSERM, IRIM, Montpellier, France.

[3]Institut de Pharmacologie et de Biologie Structurale (IPBS), Université de Toulouse, CNRS, Toulouse, France.

[4]UCB BioSciences, Bainbridge Island, WA 98109 USA

[5]Seattle Structural Genomics Center for Infectious Disease (SSGCID), Seattle, WA 98109 USA

[#]To whom correspondence should be addressed:

Tel: (+33) 4 34 35 94 47; E-mail: laurent.kremer@irim.cnrs.fr

Running title: Efficacy of NITD-916 against *M. abscessus*

There is an unmet medical need for effective treatments against *Mycobacterium abscessus* pulmonary infections, to which cystic fibrosis (CF) patients are particularly vulnerable. Recent studies showed that the antitubercular drug isoniazid is inactive against *M. abscessus* due to the incapacity of the catalase-peroxidase to convert the pro-drug into a reactive metabolite that inhibits the enoyl-ACP reductase InhA. To validate $InhA_{MAB}$ as a druggable target in *M. abscessus*, we assayed the activity of NITD-916, a 4-hydroxy-2-pyridone lead candidate initially described as a direct inhibitor of InhA that bypasses KatG biosactivation in *Mycobacterium tuberculosis*. The compound displayed low MIC values against rough and smooth clinical isolates *in vitro* and significantly reduced the bacterial burden inside human macrophages. Moreover, treatment with NITD-916 reduced the number and size of intracellular mycobacterial cords, regarded as markers of the severity of the infection. Importantly, NITD-916 significantly lowered the *M. abscessus* burden in CF-derived lung airway organoids. From a mechanistic perspective, NITD-916 abrogated *de novo* synthesis of mycolic acids and NITD-916-resistant spontaneous mutants harboured point mutations in $InhA_{MAB}$ at residue 96. That NITD-916 targets directly $InhA_{MAB}$ without activation requirements was confirmed genetically and by resolving the crystal structure of the protein in complex with NADH and NITD-916. These findings collectively indicate that $InhA_{MAB}$ is an attractive target to be exploited for future chemotherapeutic developments against this difficult-to-treat mycobacterium and highlight the potential of NITD-916 derivatives for further evaluation in pre-clinical settings.

Keywords: *Mycobacterium abscessus*, NITD-916, macrophage, organoid, InhA, mycolic acid.

M. abscessus is a rapidly growing non-tuberculous mycobacterium (NTM) of rising clinical significance and causing difficult-to-cure pulmonary diseases, particularly in patients with cystic fibrosis (CF) [1]. In these patients, infection with *M. abscessus* is often associated with a more rapid decline in lung function and the presence of *M. abscessus* can be deleterious for subsequent lung transplantation [2–4]. The *M. abscessus* complex comprises three subspecies exhibiting different clinical outcomes and drug susceptible profiles to antibiotics [5]: *M. abscessus* subsp. *abscessus* (designated hereafter *M. abscessus)*, *M. abscessus* subsp. *bolletii* (designated hereafter *M. bolletii)* and *M. abscessus* subsp. *massiliense* (designated hereafter *M. massiliense*) [6]. All three subspecies can display either a smooth (S) or a rough (R) morphotype as a consequence of the presence or absence, respectively, of surface-associated glycopeptidolipids (GPL) [7–10]. These morphological changes are linked to major phenotypic differences, including sliding motility, biofilm formation [8,9,11] or production of large bacterial cords [11,12]. S and R variants can be viewed as two representative forms of the same isolate, which can co-exist in the patient and evolve differently in response to the host immune pressure. They can also display specific pathophysiological characteristics [10]; S variants are generally less virulent than their corresponding R variants [11,13,14], the latter being more frequently associated with severe pulmonary diseases in CF patients [2,4]. In addition, different susceptibility profiles to drugs have been reported between S and R variants [15,16], thus warranting the need for evaluating compounds/drug regimens against both variants.

Due to intrinsic resistance to a wide panel of antimicrobials, including most antitubercular drugs, treatment of *M. abscessus* lung disease remains extremely challenging [17–20]. Multi-drug regimens are administered for months to years, generally comprising an oral macrolide (clarithromycin or azithromycin) and intravenously administered aminoglycosides (amikacine) and β-lactams (imipenem or cefoxitin)[21–23]. Other drugs, such as tigecycline or clofazimine, can be added to strengthen the regimen, mostly in response to toxic side effects or poor clinical response [24]. However, despite intensive chemotherapy, treatment success rates typically remain very low in the case of macrolide resistance (25-40%), which occurs in at least 40-60% of clinical isolates [25]. Thus, given the unsatisfactory performances of the current regimens, more effective drugs are required. Unfortunately, *de novo* drug discovery efforts to identify new chemical scaffolds are impeded by low hit rates [26,27], explaining why the *M. abscessus* drug pipeline focuses mainly on repurposing and reformulation of approved drugs.

In addition to mutations in genes encoding the drug targets conducting to acquired drug resistance [7,26], the widespread resistome of *M. abscessus* results also from the low permeability properties of the cell envelope, the expression of a wide range of drug-modifying enzymes, the induction of efflux pumps and the absence or dysfunctional drug-activating enzymes [17,20,28]. The latter, for instance, explains why isoniazid (INH) is totally inactive against *M. abscessus.* Indeed, it has been recently shown that the catalase-peroxidase $KatG_{MAB}$ is unable to transform INH into an active metabolite [29]. INH, the most efficient first-line anti-TB drug against actively replicating *M. tuberculosis*, remains the first choice for prophylaxis and treatment. Its biotransformation requires the catalase-peroxidase KatG [30,31] to generate an isonicotinoyl radical that reacts with NAD^+ to produce an INH-NAD adduct [32,33]. This adduct blocks the enoyl-ACP reductase (InhA) of the type II fatty acid synthase (FAS-II) [34–37], leading to the arrest of mycolic acid biosynthesis. Mycolic acids are essential and unique long-chain (C_{70}-C_{90}) α-alkyl, β-hydroxy fatty acids [35,38] and their inhibition ultimately results in mycobacterial cell death [39]. However, while being a validated drug target in *M. tuberculosis*, it remains to be established whether InhA represents an attractive target for future drug developments against *M. abscessus.*

To fill this gap, this study was undertaken to test the hypothesis whether NITD-916, a direct inhibitor of InhA that bypasses the KatG bioactivation process [40], offers potential for future chemotherapeutic developments against *M abscessus*. NITD-916 is a 4-hydroxy-2-pyridone lead candidate previously identified in a phenotypic screen against *M. tuberculosis* that exerts bactericidal activity against common INH-resistant TB clinical isolates. Herein, we aimed at assessing the activity of NITD-916 against *M. abscessus* S and R strains *in vitro,* in macrophages as well as in CF lung airway organoids and report the mechanism of action of the inhibitor in *M. abscessus*.

RESULTS

M. abscessus strains are susceptible to NITD-916 treatment *in vitro*.

To address whether InhA inhibitors bypassing KatG bioactivation can offer potential chemotherapeutic options against *M abscessus,* we first screened the literature for commercially available direct InhA inhibitors, previously validated against *M. tuberculosis* and for which *in vitro* data and efficacy in mice have been reported. This led to the 4-hydroxy-2-pyridone lead compound NITD-916 [40]. Initial experiments revealed that the *M. abscessus* $CIP104536^T$ S reference strain was particularly susceptible

to NITD-916 in CaMHB (MIC=1.56 µg/mL which is 5 µM). However, as shown previously for other compounds [41], the MIC was greatly dependent on the medium, with values of 0.195 µg/mL and 6.25 µg/mL in Sauton's medium and Middlebrook 7H9, respectively **(Table S1)**. MICs in an artificial sputum medium (ASM) containing components of the CF sputum [42] were comparable to those obtained in CaMHB.

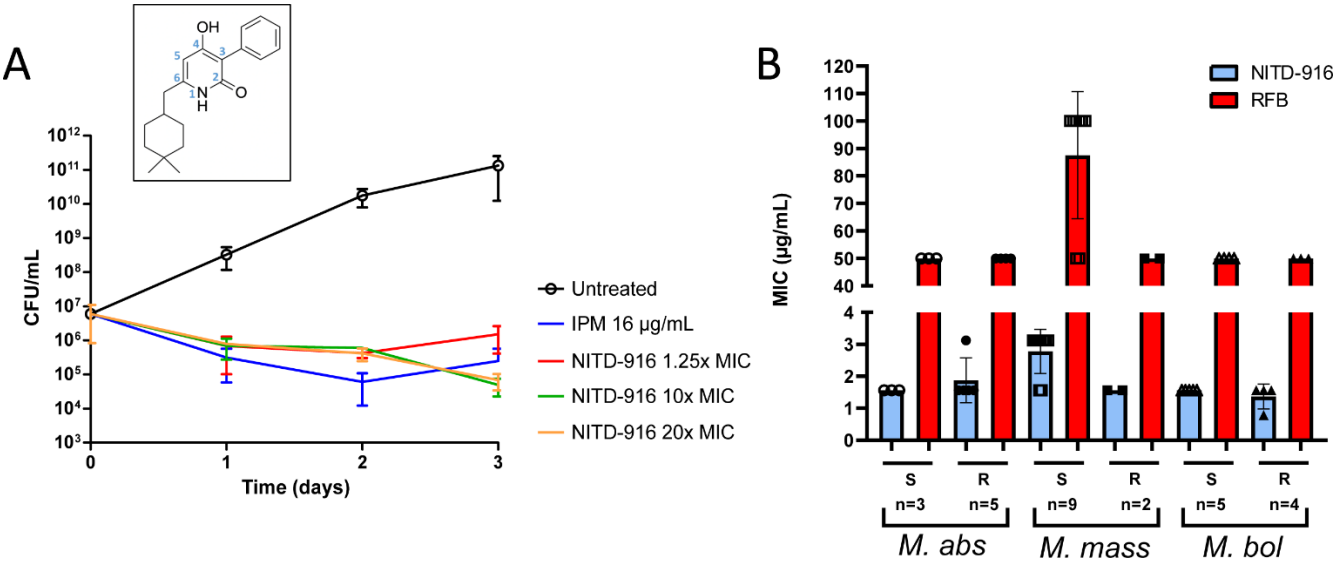

Figure 1. *In vitro* activity of NITD-916 against *M. abscessus*. (A) Cultures of *M. abscessus* CIP104536^T (S) were exposed to either 1.95, 15.6, 31.2 µg/mL NITD-916 (corresponding to 1.25x, 10x and 20x MIC) or 16 µg/mL imipenem (IPM) in CaMHB at 30 °C. At various time points, bacteria were plated on LB agar and incubated at 37 °C for 4 days prior to CFU counting. Results are expressed as the mean of 2 independent experiments in triplicates ± SD. Inset: structure of NITD-916. **(B)** MIC (in µg/mL) of NITD-916 and RFB against *M. abscessus* complex clinical isolates. MIC values were determined in CaMBH for *M. abscessus* sbsp. *abscessus* (n=8), *M. abscessus* sbsp. *massiliense* (n=11) and *M. abscessus* sbsp. *bolletii* (n=9). Data are plotted as mean values ± SD. S refers to smooth strains; R refers to rough strains.

To determine the effect of the compound in broth culture, exponentially-growing *M. abscessus* was exposed to increasing concentrations of NITD-916, corresponding to 1.25x, 10x and 20x MIC. This resulted in a noticeable growth inhibition **(Fig. 1A)**. However, the number of colony-forming units (CFU) remained relatively stable at the lowest concentration tested during the 3 days of treatment and comparable to those in the inoculum, suggesting a bacteriostatic effect. In addition, the killing effect was not concentration-dependent, at least during the first two days of treatment. An additional 1-Log drop was observed after 3 days with 10x or 20x MIC. At these concentrations, NITD-916 resulted in a

growth inhibitory effect comparable to the one of imipenem (IPM) used at the MIC (16 µg/mL), a known β-lactam antibiotic active against *M. abscessus* [43]. In addition, while overexpression of KatG from *M. tuberculosis* restored susceptibility to INH in *M. abscessus* carrying pSMT3-*katG*$_{MTB}$-*tdTomato* as previously reported [29], the MIC of NITD-916 remained unchanged in this strain as compared to its parental progenitor **(Table S2)**. This implies that, in contrast to INH, the activity of NITD-916 is KatG-independent in *M. abscessus*.

The potency of NITD-916 was next assayed using a representative panel of clinical isolates from CF patients or non-CF patients, comprising 8 *M. abscessus* subspecies *abscessus*, 11 *M. abscessus* subspecies *massiliense* and 9 *M. abscessus* subspecies *bolletii* strains. All these strains were susceptible to NITD-916, similarly to the CIP104536^T reference strains **(Fig. 1B)** and, in general, the MIC of R and S strains were similar, altough slight variations were observed between the *M. massiliense* strains. The MIC values of NITD-916 were found to be much lower than those of rifabutin (RFB), included as a control drug [41]. Overall, these results demonstrate that NITD-916 exerts potent activity on the *M. abscessus* complex and is equally active against strains isolated from CF and non-CF patients.

NITD-916 inhibits intramacrophage growth of *M. abscessus*. To assess whether NITD-916 is active against *M. abscessus* in a macrophage infection model, we next compared the intracellular efficacy of the compound in human THP-1 macrophages infected with either CIP104536^T S and R variants after 1 and 3 days of exposure to the compound **(Fig. 2A** and **2B)**. First, the cytotoxicity of NITD-916 against THP-1 cells was investigated after 1 and 3 days of exposure to the compound. **Fig. S1** clearly shows that NITD-916 exerts cytotoxicity only at very high concentrations (>100 µg/mL) at both time points. NITD-916-induced cytotoxicity was intermediate between INH (no cytotoxicity at 100 µg/mL) and RFB (100% macrophage killing at 100 µg/mL) after 3 days of exposure to each drug. These results indicate that NITD-916 exhibits very little toxicity at concentrations below 100 µg/mL and, based on these results, all subsequent macrophage studies were conducted with 1.56, 15.6 and 31.2 µg/mL NITD-916, corresponding to 1x, 10x and 20x MIC. RFB was included as a positive control at 12.5 µg/mL, a concentration at which it significantly reduces the intracellular burden [41]. DMSO-treated macrophages were added as a negative control for intracellular bacterial replication. At 0, 1 and 3 days post-infection (dpi), macrophages were lysed and plated to determine the intracellular bacterial burden after drug treatment. Similarly to the DMSO condition, exposure of macrophages to NITD-916 at 1x MIC failed to

inhibit intramacrophage growth of *M. abscessus* CIP104536^T S **(Fig. 2A)** and CIP104536^T R **(Fig. 2B)** at 1 and 3 dpi. In contrast, exposure to 10x MIC strongly decreased the intracellular bacterial loads at 1 dpi and this effect was further amplified at 3 dpi in both strains. Interestingly, there was no difference between 10x and 20x MIC of NITD-916, and the CFU counts were comparable to those in the inoculum (Day 0), similarly to what was observed in liquid cultures **(Fig. 1A)**. In addition, the NITD-916 susceptibility profile for the S variant at 1 and 3 dpi was comparable to that of the R variant, with a ~2 Log reduction in the CFU counts at day 3, reaching the same level of inhibition than RFB **(Fig. 2A** and **B)**.

We further explored the activity of NITD-916 against S and R clinical isolates of the *M. abscessus* complex within THP-1 macrophages. Supporting our previous observations with the CIP104536^T reference strains, we found that NITD-916 was very active against all *M. abscessus* subspecies tested within macrophages at 1 and 3 dpi when compared to day 0 and DMSO treatment, irrespective of S and R morphotype: *M. abscessus* 2069 (S) **(Fig. 2C),** *M. abscessus* 2524 (R) **(Fig. 2D)**, *M. massiliense* 179 (R) **(Fig. 2E),** *M. massiliense* 120 (S) **(Fig. 2F)**, *M. bolletii* 112 (R) **(Fig. 2G)** and *M. bolletii* 108 (R) **(Fig. 2H)**. In all cases, the optimal activity was reached in the presence of 10x MIC of NITD-916. Overall, these results indicate that NITD-916 is a potent intracellular growth inhibitor of *M. abscessus*.

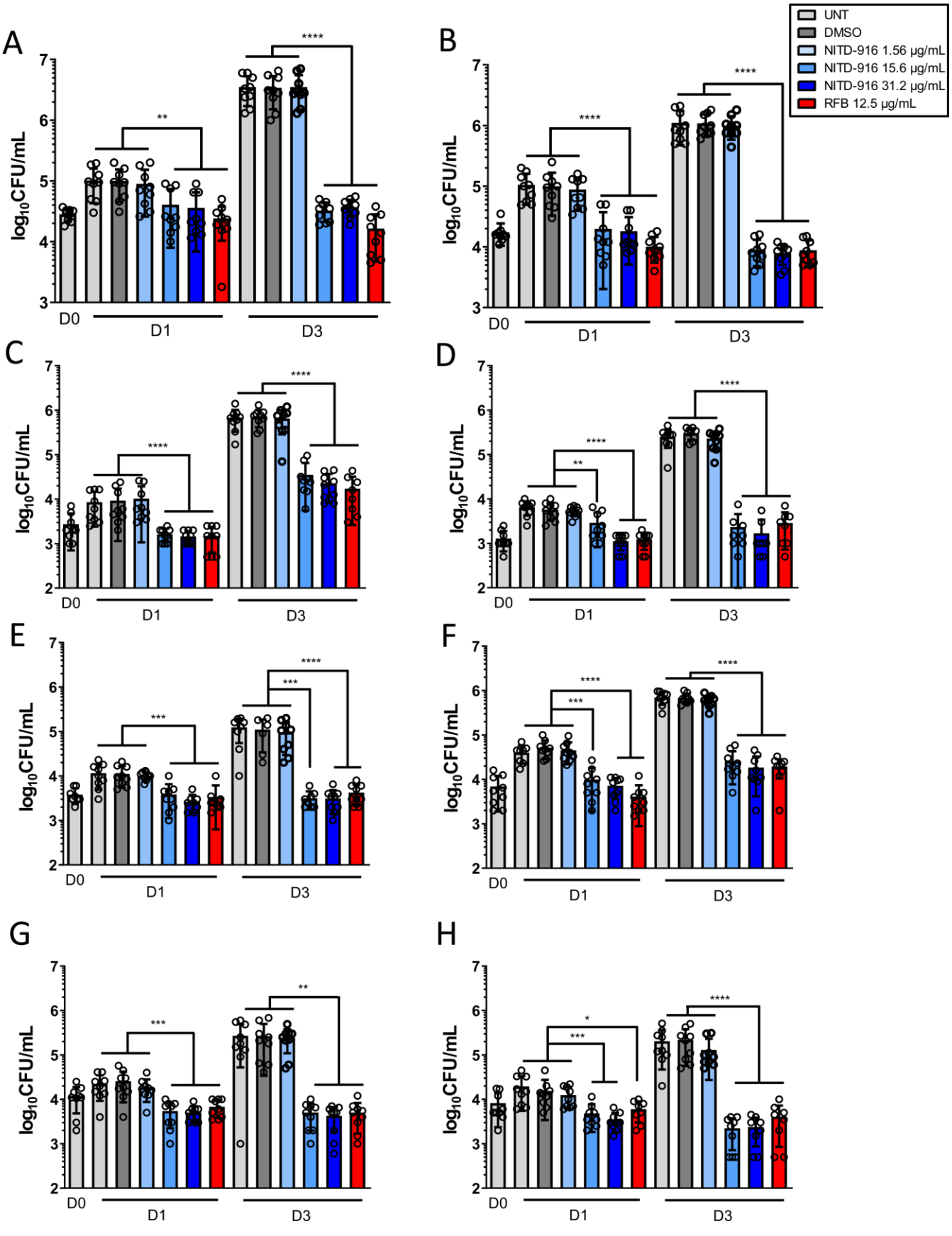
A
B
C
D
E
F
G
H
UNT
DMSO
NITD-916 1.56 µg/mL
NITD-916 15.6 µg/mL
NITD-916 31.2 µg/mL
RFB 12.5 µg/mL
log10CFU/mL
D0
D1
D3

Figure 2. Intracellular activity of NITD-916 on *M. abscessus* complex-infected THP-1 cells. Macrophages were infected with *M. abscessus* reference strains and clinical isolates (MOI of 2:1) for 4 hrs prior to treatment with 250 µg/mL AMK for 2 hrs to kill extracellular bacteria. Cells were then exposed to either NITD-916 or to RFB at the indicated concentrations. Untreated (UNT) or DMSO-exposed cells were included as controls. CFU were determined at 0, 1 and 3 days post-infection. The various strains tested and morphotypes are as follows: **(A)** *M. abscessus* CIP104536^T (S) ; **(B)** *M. abscessus* CIP104536^T (R) ; **(C)** *M. abscessus* 2069 (S) ; **(D)** *M. abscessus* 2524 (R) ; **(E)** *M. massiliense* 179 (R) ; **(F)** *M. massiliense* 120 (S) ; **(G)** *M. bolletii* 112 (R) ; **(H)** *M. bolletii* 108 (R). Data of 3 independent experiments in triplicates were analyzed with a Mann-Whitney *t* test. *, $P \leq 0.05$; **, $P \leq 0.01$; *** $P \leq 0.001$; ****, $P \leq 0.0001$.

Intracellular *M. abscessus* loads and cording are reduced by NITD-916.

THP-1 macrophages were infected with red fluorescent *M. abscessus* strains expressing TdTomato and exposed to either DMSO, NITD-916 or RFB, stained with anti-CD63 and DAPI and observed under the microscope. A quantitative analysis highlighted a marked reduction in the percentage of *M. abscessus* R-infected cells treated with NITD-916 at 10x MIC (while no effect was observed at 1x MIC), which was comparable to the effect observed with 12.5 µg/mL RFB at 1 dpi **(Fig. 3A)**. This trend was even more pronounced at 3 dpi. Since the proportion of NITD-916-treated infected cells remained similar to the one at day 0, this suggests that the compound is very likely to be bacteriostatic inside the macrophage. Similar results were found when macrophages were infected with *M. abscessus* S **(Fig. S2A**). Representative immuno-fluorescent fields illustrate the reduced number of macrophages infected with the R **(Fig. 3B)** or S **(Fig. S2B)** variants treated with NITD-916 at 1 and 3 dpi, as compared to the untreated or DMSO-treated control cells.

Macrophages infected with the R variant were then classified into three classes as judged by their bacterial load content: poorly infected (<5 bacilli/cell), moderately infected (5-10 bacilli/cell) and heavily infected (>10 bacilli/cell). Bacteria-containing macrophages were then individually observed under the microscope and scored for their belonging to one of the three categories. The quantitative analysis indicates that treatment with NITD-916 at 10x MIC or RFB significantly reduces the percentage of heavily infected THP-1 cells and increases the proportion of the poorly infected category, as compared to the untreated or DMSO-treated cells at 1 and 3 dpi **(Fig. 3C)**, with ≈20% of the infected bacilli belonging to the heavily infected category and ≈50% associated with the poorly infected category at 3 dpi. Analysis performed on macrophages infected with the S variant generated a similar category

pattern, **(Fig. S2C).** Collectively, these data indicate that NITD-916 enters THP-1 macrophages and impedes bacterial replication of both *M. abscessus* S and R variants.

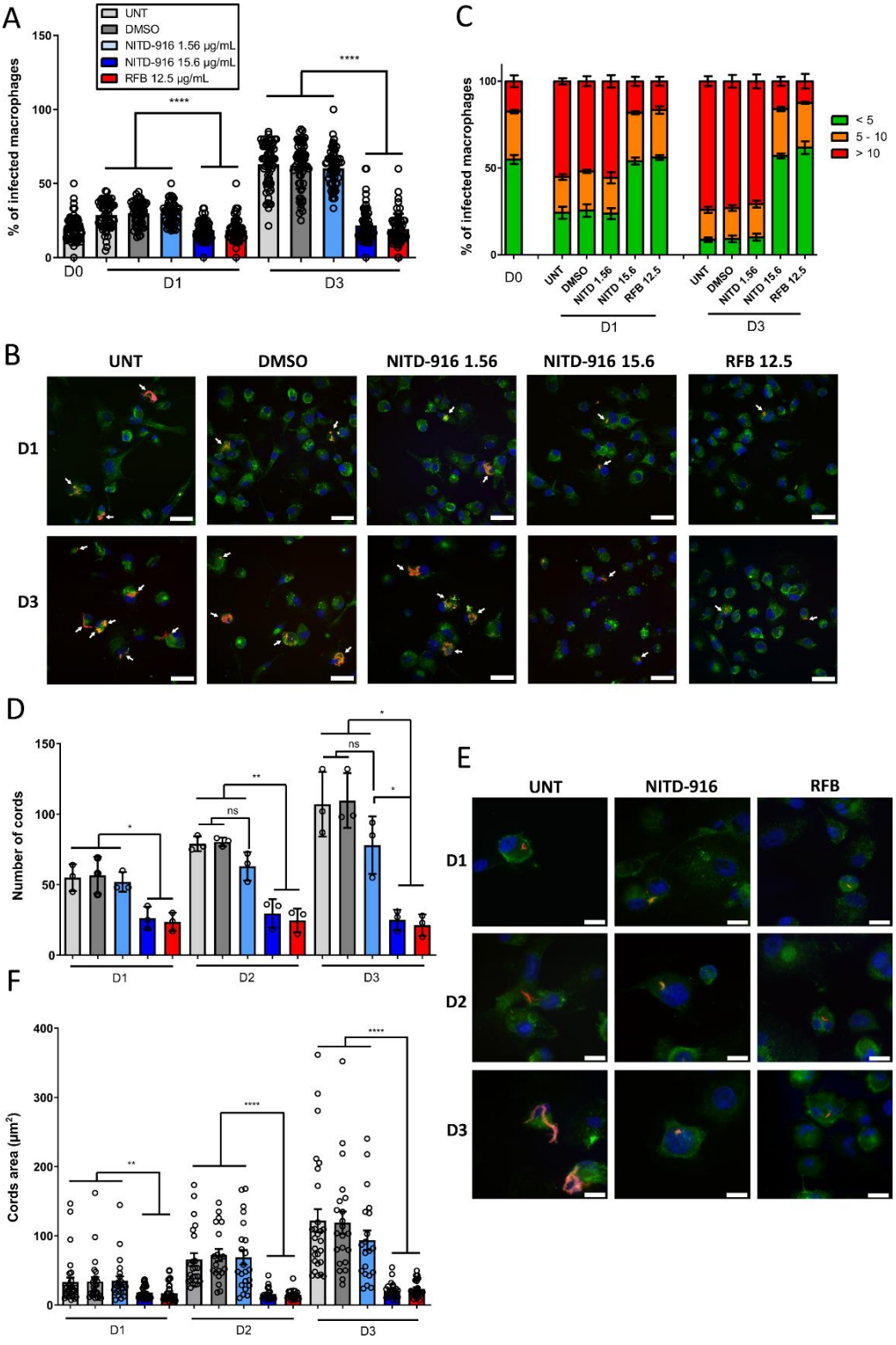

Figure 3. Effect of NITD-916 treatment on intracellular *M. abscessus* loads and cording. (A) Percentage of infected THP-1 macrophages at 0, 1 and 3 days post-infection with *M. abscessus* CIP104536^T (R) (MOI of 2:1) in the absence (UNT) of antibiotics or presence of NITD-916 (1.56 µg/mL and 15.6 µg/mL) or RFB (12.5 µg/mL). DMSO-exposed cells were included as controls. Results are expressed as mean values ± SD for three independent experiments with 30 fields per condition. Data were analyzed using the *t* test. ****, $P \leq 0.0001$. **(B)** Representative immuno-fluorescent fields were taken at 1 and 3 days post-infection showing macrophages infected with *M. abscessus* CIP104536^T (R) expressing TdTomato (red) in the absence of antibiotics (UNT) or in the presence of NITD-916 (1.56 µg/mL and 15.6 µg/mL) or RFB (12.5 µg/mL). DMSO-exposed cells were included as controls. The surface and the endolysosomal system of the macrophages were detected using anti-CD63 antibodies (green). The nuclei were stained with DAPI (blue). White arrows indicate individual or mycobacterial aggregates. Scale bar, 50 µm. **(C)** Percentage of macrophages categories infected with different number of bacilli (<5 bacilli/cell, 5 to 10 bacilli/cell, >10 bacilli/cell). The categories were counted at 0, 1 and 3 days post-infection in the absence of antibiotics or in the presence of NITD-916 (1.56 µg/mL and 15.6 µg/mL) or RFB (12.5 µg/mL). Untreated (UNT) or DMSO-exposed cells were included as controls. Data are mean values ± SD for three independent experiments performed in triplicates. **(D)** Total number of intracellular cords displayed in 30 fields at 1, 2 and 3 days post-infection. Results are expressed as mean values ± SD for three independent experiments. Data were analyzed using the two-tailed nonpaired *t* test. *, $P \leq 0.05$; **, $P \leq 0.01$ **(E)** Representative images of intracellular cords at macrophage 1, 2 and 3 days post-infection. Cords are in red, the macrophage surface is green and the nucleus in blue as in **(B)**. Scale bar, 20 µm. **(F)** Size of the intracellular cords (expressed by the area in µm^2) displayed in 10 fields. Results are expressed as mean values ± SD for three independent experiments, each symbol represents the size of a cord (n=30). Data were analyzed using the Mann-Whitney *t* test. **, $P \leq 0.01$; ****, $P \leq 0.0001$.

In contrast to the S variant, strains exhibiting a R morphotype are typified by increased bacterial clumping and R bacilli remain aggregated to generate compact colonies comprising corded structures on agar, in broth medium and inside macrophages [8,12,14,41]. **Fig. 3D** clearly illustrates that, upon infection with TdTomato-expressing *M. abscessus* R, the total number of intracellular cords displayed in 30 fields was significantly reduced in the presence of NITD-916 at 10x MIC or 12.5 µg/mL RFB when compared to untreated or DMSO-treated cells and this effect was maintained at 1, 2 and 3 dpi. The effect was not significant at 1x MIC. Representative images of intracellular cords show the kinetics of cord formation at 1, 2 and 3 dpi **(Fig. 3E)**. While very small in size at 1dpi, cord continue to elongate at 2 dpi and 3 dpi, often leading to structure capable of extruding out the cells at 3 dpi, presumably participating in macrophage killing. In the presence of drugs (NITD-916 or RFB), there was a clear reduction in size of the cords as compared to the untreated cells. This effect is supported by a quantitative analysis of the cord surface area (expressed in µm^2). While control cords continue to increase in size over time (reaching a surface area >100 µm^2), their size remained constant (≈20 µm^2) upon exposure to NITD-916

or RFB **(Fig. 3F)**. Together, these results indicate that NITD-916 is highly effective in reducing the number and size of *M. abscessus* cords, thought to affect the outcome of the infection.

NITD-916 reduces *M. abscessus* loads in human airway organoids.

Lung airway organoids (AO) from healthy individuals have recently been developed to study the early steps of interaction between *M. abscessus* and the airway [44]. In this biological model where mycobacteria are injected in AO, *M. abscessus* was found to actively replicate over 7 days in the lumen and this was accompanied by reduced expression of mucin genes, usually participating in the clearance of pulmonary pathogens [44]. Moreover, AOs derived from CF patients were characterized by low CFTR activity and enhanced mucus accumulation and the subsequent injection of *M. abscessus* in these 3D structures revealed the production of biofilms formed by the S variant and serpentine cords formed by the R variant [45]. Importantly, both variants replicated more efficiently in CF AOs than in AOs derived from healthy lungs, thus highligthing the relevance of this model to study the pathogenesis of *M. abscessus* and to test the therapeutic potential of compounds in a system that recapitulates a CF environment [45]. As illustrated in **Fig. 4A**, CF-derived AOs were injected with the *M. abscessus* S and R variants expressing Wasabi and drug treatment was commenced two hours later with NITD-916 at 1.56 µg/mL or 15.6 µg/mL and with RFB at 12.5 µg/mL, included as a control drug. After 3 days of treatment, fluorescence microscopy showed high bacterial loads in AOs left untreated or exposed to 1.56 µg/mL NITD-916, while exposing the AOs to the 15.6 µg/mL dose significantly reduced the green fluorescence signal, similarly to the RFB treatment **(Fig. 4B)**. AOs were then lysed at 3 dpi and plating the lysates on agar indicated a 2-Log increase in the CFU of *M. abscessus* S in the untreated control or in the presence of 1.56 µg/mL NITD-916 **(Fig. 4C)**. In contrast, treatment with either 15.6 µg/mL NITD-916 or 12.5 µg/mL RFB was associated by a striking decrease in the CFU counts, at levels similar to those found in the inoculum (Day 0) **(Fig. 4C)**. Very similar results were observed for *M. abscessus* R-containing AOs **(Fig. 4D** and **4E)**. Overall, these results clearly indicate that NITD-916 is active in CF patient-derived AOs characterized with severe CF airway dysfunction and susceptibility to *M. abscessus* infection.

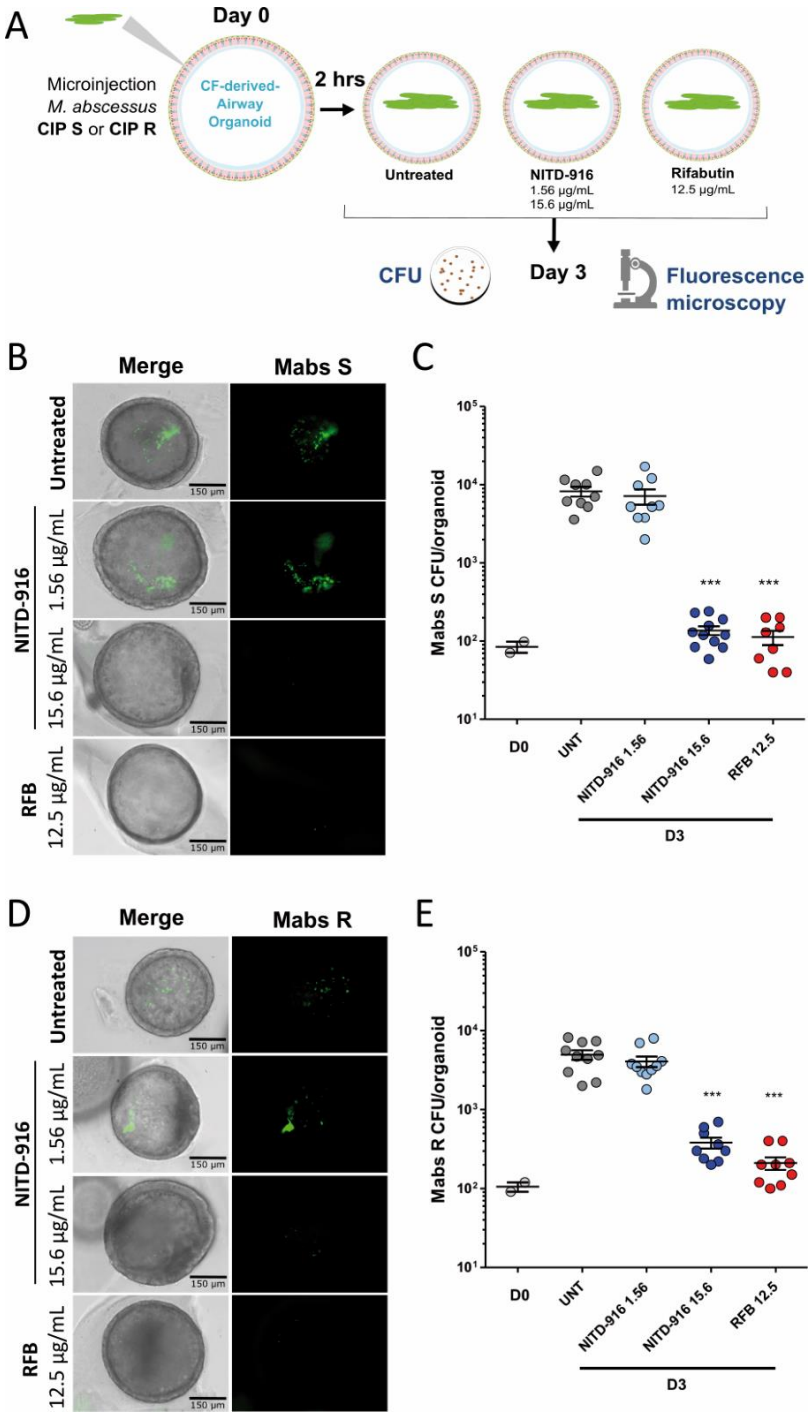

Figure 4. Activity of NITD-916 in *M. abscessus*-infected CF-derived airway organoids. (A) A generalized schematic showing the experimental design. Representative images **(B, D)** and corresponding bacterial loads determined by CFU counting **(C, E)** of CF-derived airway organoids at 3 days post-infection with *M. abscessus* S **(B, C)** or R **(D, E)** expressing Wasabi in the presence of absence of treatment: untreated groups (S n=9; R n=10), treated with NITD-916 at 1.56 µg/mL (S n=9; R n=10), NITD-916 at 15.6 µg/mL (S n=11; R n=9) or RFB at 12.5 µg/mL (S n=8; R n=9). Graphs show means ± SD of two independent experiments. Each dot represents one organoid. Data were analyzed using the Mann-Whitney *t* test. ***, $P \leq 0.001$.

Mutations in *inhA*$_{MAB}$ confer high resistance levels to NITD-916.

Mutations in *inhA* coding for the enoyl-ACP reductase of the type II fatty acid synthase have been reported previously in *M. tuberculosis* mutants resistant to NITD-916 [40]. To get insights into the mode of action of NITD-916 in *M. abscessus*, a genetic approach was conducted involving the selection of spontaneous NITD-916-resistant mutants derived from either the smooth (S) or rough (R) *M. abscessus* parental strains on agar supplemented with 15.6 µg/mL NITD-916 (10x MIC) at frequencies estimated to $2.3x10^{-7}$ (S resistant strains) and $2.4x10^{-6}$ (R resistant strains). MIC determination of four individual colonies for each morphotype confirmed their high resistant levels (MIC>100 µg/mL) against NITD-916 while remaining susceptible to RFB and ETH **(Table 1)**. Sequencing the *inhA*$_{MAB}$ (*MAB_2722c*) locus identified single nucleotide polymorphisms (SNPs) across the different resistors, leading to amino acid replacements at position 96. In the S resistors, NITD916^{R1} and NITD916^{R4}, Gly96 was replaced by a Val residue while in NITD916^{R2} and NITD916^{R3} Gly96 was replaced by a Ser residue. All four mutants derived from the R variant (NITD916^{R5} to NITD916^{R8}) harboured a G96V amino acid exchange **(Table 1)**. As shown for NITD916^{R2}, resistance to NITD-916 was independent of the medium **(Table S1)**.

Table 1. Characteristics of NITD-916 spontaneous resistant mutants of *M. abscessus.* MIC (µg/mL) were determined in CaMHB. Resistant strains were derived from either the smooth (S) or rough (R) *M. abscessus* CIP104536^{T} parental strains on LB agar supplemented with 15.6 µg/mL NITD-916 (10x MIC). Single-nucleotide polymorphism (SNP) in *inhA*$_{MAB}$ (*MAB_2722c*) and corresponding amino acid (AA) changes as well as frequency of mutation are indicated.

	MIC (µg/mL)			Mutation in *inhA*$_{MAB}$		
Strain	**NITD-916**	**RFB**	**ETH**		**AA change**	**Frequence of mutation**
CIP104536^{T} (S)	1.56	100	25			
NITD916^{R1}	>100	50	12.5	G287T	G96V	$2.3x10^{-7}$
NITD916^{R2}	>100	100	25	G286A	G96S	$2.3x10^{-7}$
NITD916^{R3}	>100	50	50	G286A	G96S	$2.3x10^{-7}$
NITDR916^{R4}	>100	50	25	G287T	G96V	$2.3x10^{-7}$
CIP104536^{T} (R)	1.56	12.5	25			
NITD916^{R5}	>100	12.5	12.5	G287T	G96V	$2.4x10^{-6}$
NITD916^{R6}	>100	12.5	25	G287T	G96V	$2.4x10^{-6}$
NITD916^{R7}	>100	25	25	G287T	G96V	$2.4x10^{-6}$
NITD916^{R8}	>100	12.5	25	G287T	G96V	$2.4x10^{-6}$

To validate *inhA*$_{MAB}$ as a specific target of NITD-916, wild-type and mutated *inhA*$_{MAB}$ alleles were cloned in frame with a HA-tag under the control of the constitutive *hsp60* promoter to allow overexpression of the wild-type and mutated versions of the protein. The resulting constructs, pMV261-*inhA*$_{MAB,}$ pMV261-*inhA*$_{MAB}$*(G96V)* and pMV261-*inhA*$_{MAB}$*(G96S)* were introduced in both S and R variants and expression of the different InhA$_{MAB}$ variants was confirmed by Western blotting using anti-HA antibodies, while levels of the Ag85 complex remain constant **(Fig. 5A)**. Whereas overproduction of the wild-type proteins did not significantly alter the MIC values as compared to the parental progenitors (two-fold effect), overproduction of InhA$_{MAB}$(G96V) or InhA$_{MAB}$(G96S) resulted in 8- to 32-fold upshift in the MIC level **(Table 2)**. These effects were specific to NITD-916 as the MIC of RFB against the same recombinant strains were comparable to those of the parental progenitors **(Table 2)**. This indicates that transferring the single point mutations identified in the NITD-916 spontaneous resistant mutants into a susceptible strain is sufficient to confer high resistance levels to NITD-916.

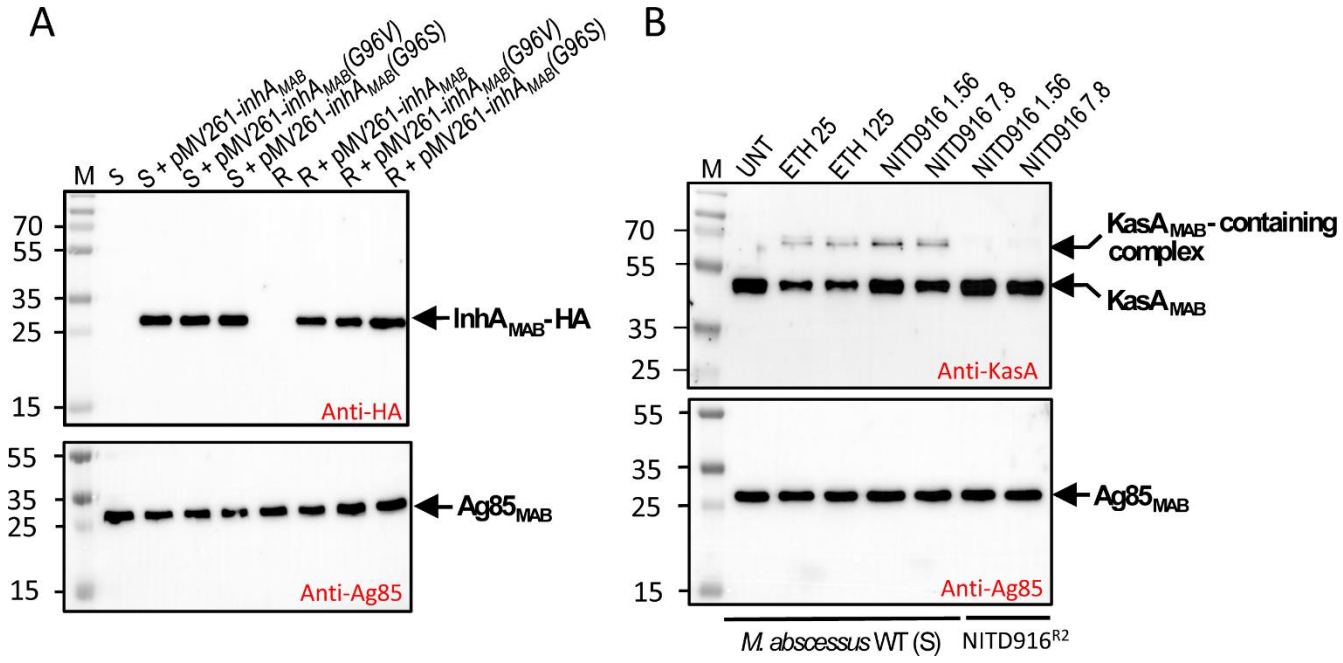

Figure 5. Overexpression of InhA$_{MAB}$ variants in *M. abscessus* S and R strains. (A) Western blots using antibodies against the HA-epitope (upper panel) and the Ag85 complex (lower panel) as loading control were done to assess the expression levels of the InhA$_{MAB}$ variants in various strains overproducing either InhA$_{MAB}$(WT), InhA$_{MAB}$(G96V) or InhA$_{MAB}$(G96S). Equal amounts of total lysates (10 µg) of each strain were separated on a 12% SDS-PAGE. **(B)** Wild-type *M. abscessus* CIP104536^{T} (S) and NITD916^{R2} strains were grown in CaMBH and exposed for 9 hrs with increasing concentrations of ethionamide (ETH) or NITD-916 at concentrations corresponding to 1x and 5x MIC. Equal amounts of total lysates (10 µg) of each strain were separated on a 12% SDS-PAGE and probed with anti-KasA (upper panel) anti-Ag85 complex (lower panel) antibodies (used as loading control).

Table 2. MIC (μg/mL) of NITD-916 and RFB determined in CaMHB at 30 °C against *M. abscessus* overexpressing wild-type and mutated *inhA$_{MAB}$ (MAB_2722c*) alleles.

Strain	NITD-916	RFB
CIP104536^T (S)	**1.56**	**50**
S + pMV261-*inhA$_{MAB}$*	3.12	50
S + pMV261-*inhA$_{MAB}$(G96V)*	25	50
S + pMV261-*inhA$_{MAB}$(G96S)*	50	50
CIP104536^T (R)	**1.56**	**12.5**
R + pMV261-*inhA$_{MAB}$*	3.12	12.5
R + pMV261-*inhA$_{MAB}$(G96V)*	12.5	12.5
R + pMV261-*inhA$_{MAB}$(G96S)*	50	12.5

It was previously reported that isoniazid, diazaborine or ethionamide (ETH) induced the production of a KasA-containing complex in *M. smegmatis* and that formation of this complex is a consequence of InhA inhibition while other FAS-II inhibitors such as thiolactomycin or isoxyl, inhibiting KasA and the HadABC dehydratase, respectively, fail to induce this complex [46]. Thus, we inquired whether NITD-916 induces this complex in *M. abscessus* by probing crude lysates from cultures exposed to 1x and 5x MIC NITD-916 with anti-KasA antibodies. **Fig. 5B** reveals, in addition to free KasA$_{MAB}$, the presence of an additional immmunoreactive band at both concentrations. This protein co-migrated with a protein also present in the ETH-treated lysates (used as a positive control of InhA$_{MAB}$ inhibition) while absent in the untreated sample. Importantly, this KasA-containing complex was not induced in strain NITD916^{R2} resistant to NITD-916, presumably because the G96S mutation in InhA$_{MAB}$ renders the enzyme insensitive to NITD-916. Overall, these results suggest that InhA$_{MAB}$ is the primary target of NITD-916 in *M. abscessus* and that its inhibition lead to the induction of a KasA-containing complex.

NITD-916 inhibits *de novo* mycolic acid biosynthesis in *M. abscessus*.

In contrast to *M. tuberculosis*, *M. abscessus* does not synthesize oxygenated mycolic acids but produces exclusively α and α' mycolates, corresponding to long-chain (C_{77-79}) and short chain (C_{62-64}) mycolic acid subspecies, respectively [47]. To interrogate whether NITD-916 inhibits *de novo* synthesis of mycolic acids, [^{14}C]-labeled lipids were extracted from wild-type *M. abscessus* cultures treated with increasing concentrations of NITD-916 prior to labelling with 1 μCi/mL [2-^{14}C]acetate. Mycolic acid methyl esters (MAMEs) and fatty acid methyl esters (FAMEs) were then separated by thin-layer chromatography (TLC). Synthesis of both α and α' mycolates was dramatically affected in a dose-dependent manner **(Fig.**

6A). *De novo* synthesis was almost completely abrogated in the presence of 1.56 µg/mL (1x MIC). Ethionamide (ETH), a drug known to target InhA and whose biotransformation is dependent on EthA instead of KatG [48] was included as a positive control. However, due to the elevated MIC of ETH against *M. abscessus* (25 µg/mL), only partial inhibition was achieved at the concentrations tested. Importantly, that no inhibition was noticed in the production of fatty acid methyl esters (FAMEs) during treatment with NITD-916, indicates that, like ETH or INH, NITD-916 specifically inhibits FAS-II rather than FAS-I, as expected for InhA-dependent inhibition.

We next addressed whether resistance to NITD-916 can be linked to an unaltered mycolic acid profile in strains caryring mutations in $InhA_{MAB}$. Supporting this hypothesis, mycolic acid biosynthesis in strain $NITD916^{R2}$ (carrying G96S point mutation) was much more refractory to inhibition by NITD-916 as compared to the wild-type progenitor **(Fig. 6B)**. Collectively, these biochemical data underline a mode of action that results in the abolishment of mycolic acid biosynthesis by targeting $InhA_{MAB}$.

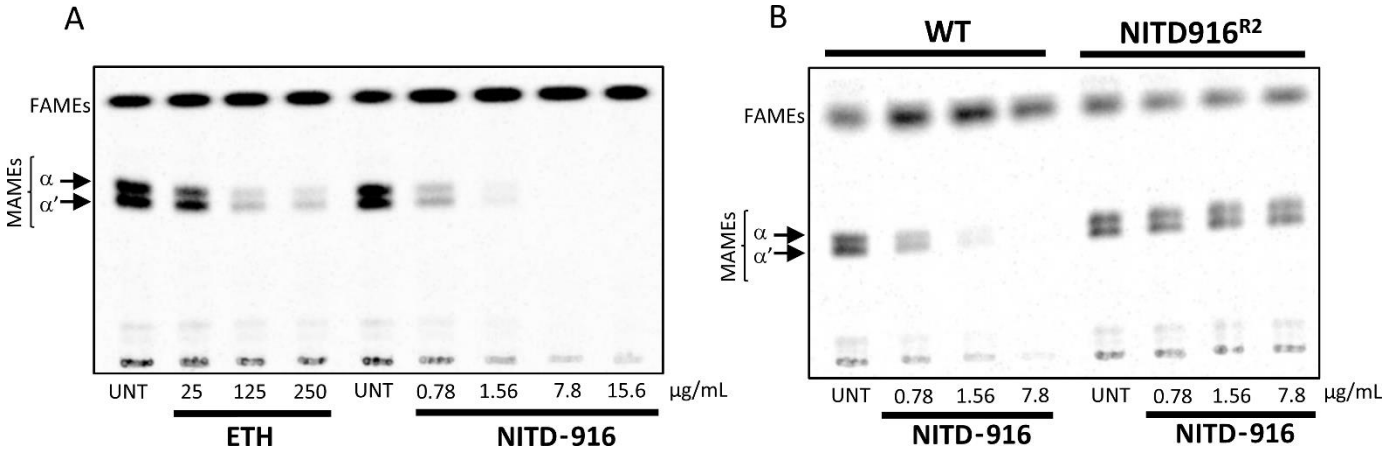

Figure 6. Inhibition of mycolic acid biosynthesis by NITD-916 in *M. abscessus.* (A) Dose-response effects of ethionamide (ETH) and NITD-916 in *M. abscessus* $CIP104536^T$ (S). The inhibitory effect on the incorporation of [2-^{14}C]acetate was assayed by exposing cultures to increasing concentrations of ETH or NITD-916 for 1 hr prior to labelling for another 2 hrs at 37 °C under shaking. The corresponding radiolabelled FAMEs and MAMEs were extracted. Equal counts (50,000 cpm) were loaded onto a TLC plate and lipids were developed in petroleum ether/acetone (95/5, v/v). **(B)** Mutant $NITD916^{R2}$ is refractory to mycolic acid inhibition by NITD-916. *M. abscessus* $CIP104536^T$ (S) and its derivative $NITD916^{R2}$ were exposed to concentrations corresponding to 0.5x, 1x and 5x MIC of NITD-916, labeled and subjected to lipid extraction and analysis as in **(A)**.

Structural basis for $InhA_{MAB}$ inhibition by NITD-916.

To demonstrate direct target engagement, we obtained a 1.45 Å resolution crystal structure of $InhA_{MAB}$ bound to NITD-916 and NAD **(Fig. 7A** and **Table S3)**. As described above, resistance mutants arose at

residue Gly96. In our structure, the C_α of Gly96 residues is in proximity to the 2'-hydroxyl of the NMN portion of NAD as well as the phenyl moiety of NITD-916 **(Fig. 7A**). Mutation of this residue would cause a steric clash with the phenyl ring of NITD-916, potentially explaining the G96S and G96V resistance mutations. Modifying the phenyl ring of NITD-916 could potentially result in molecules which overcome resistance at G96. However, given the proximity to the 2'-hydroxyl of the NMN portion of NAD, mutation of G96 could also cause loss of InhA specific activity and these resistance mutations may not arise in a clinical setting. Residues interacting with NITD-916 are indicated in **Fig. 7A**.

Overall, our structure is similar to a previously obtained 3.2 Å resolution structure of $InhA_{MTB}$ bound to NITD-916 and NAD [40] **(Fig. 7B)**. The 4-hydroxy-2-pyridin-2-one moiety stacks on top of the nicotinamide ring, presumably where the unsaturated portion of the substrate binds, whereas the 4,4-dimethylcyclohexyl moiety projects into the hydrophobic cavity presumably where the lipid portion of the substrate binds. Thus, NITD-916 appears to be a direct substrate competitor. In addition, there appears to be some induced fit upon NITD-916 binding when compared to our structures of the $InhA_{MAB}$ apoenzyme (1.75 Å resolution) or the holoenzyme (1.85 Å resolution) **(Fig. 7C)**. Our structures of $InhA_{MAB}$ in the apoenzyme, holoenzyme, and NITD-916 inhibited state show that the residues spanning Thr196 through Gly212 move considerably in response to the ligand-bound state. In the $InhA_{MAB}$ apoenzyme state these residues form a β-hairpin turn and generate an open catalytic cavity. In the holoenzyme state, these residues change to an α-helix which packs tightly against the co-factor and generate a narrow substrate binding cleft. In the inhibited form, this new α-helix moves away from the co-factor to accommodate the binding of NITD-916. These residues and to a lesser extent α6 (numbering using the apoenzyme state) are the only major conformational changes that occur between the different states. Similar conformational changes have been observed previously for $InhA_{MTB}$ substrates (e.g. PDB ID 1BVR [49]) and other inhibitor-bound structures (e.g. PDB ID 1P44 [50]).

To complement the crystallography work and gain some understanding of the effects of the inhibitor NITD-916 on the thermal stability of $InhA_{MAB}$, we performed differential scanning fluorimetry (DSF). Apoenzyme $InhA_{MAB}$ had a melting temperature of 39.3 °C **(Table S4** and **Fig. S3)**. Incubation with the co-factor NAD to generate the holoenzyme resulted in a modest increase in melting temperature to 39.8 °C (ΔTm = 0.5 °C). Generation of the inhibited complex of $InhA_{MAB}$ with NAD and NITD-916 resulted in a large increase in the melting temperature to 54.0 °C (ΔTm = 14.7 °C relative to apo or 14.2 °C

relative to NAD alone). Although such stability measurements are not directly correlated with affinity, significant stabilization can be indicative of potency in biochemical experiments.

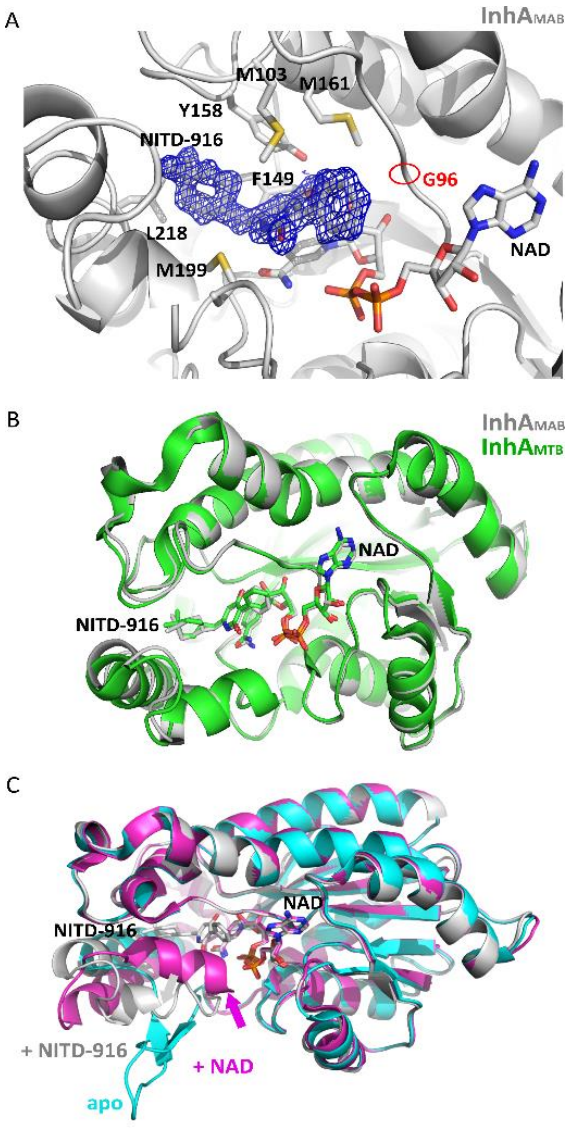

Figure 7. Structural basis of inhibition of *M. abscessus* InhA by NITD-916. (A) Crystal structure of *M. abscessus* InhA bound to NITD-916 and NAD solved at 1.45 Å resolution. For simplicity only one protomer of the tetrameric structure is shown. The protein is depicted as gray ribbons and the inhibitor NITD-916 and co-factor NAD are shown rendered in sticks. The final $2|F_o|-|F_c|$ map for NITD-916 is shown in blue mesh contoured at 1.0 sigma. The site of resistance mutations G96 is circled in red and other residues which interact with NITD-916 are labeled and shown with their side chains rendered in sticks. **(B)** Overlay of the crystal structures of $InhA_{MAB}$ bound to NITD-916 and NAD depicted as above and $InhA_{MTB}$ bound to NITD-916 and NAD shown in green ribbons for the protein and green carbon sticks for the inhibitor and co-factor. **(C)** Overlay of the crystal structure of $InhA_{MAB}$ in the apoenzyme state shown in cyan ribbons, the holoenzyme state bound to NAD in magenta with NAD in magenta sticks, and the inhibited state bound to NAD and NITD-916 in gray as in the upper panels. The loop spanning residues Thr196 through Gly212 moves significantly upon co-factor and inhibitor binding.

DISCUSSION

The success rate of *M. abscessus* pulmonary disease treatment remains very poor despite prolonged, multidrug antibiotherapy with an important risk of severe secondary effects, emphasizing the rapid need for more effective treatments [26]. While mycolic acids represent essential cell wall components in mycobacteria and are the primary target of INH and ETH in *M. tuberculosis*, none of the current drugs used in clinical settings against *M. abscessus* infections are hitting mycolic acid biosynthesis. However, recent studies have emphasized that this metabolic pathway represents an attractive niche for druggable targets in *M. abscessus*. First, thiacetazone has proven to bind to the HadA component of the FAS-II HadABC dehydratase complex, leading to mycolic acid inhibition in *M. tuberculosis* [51] and thiacetazone derivatives exhibited potent activity against the *M. abscessus* complex [52]. Second, a large number of hits against *M. abscessus* have recently been shown to inhibit the transport of mycolic acids across the membrane by targeting the MmpL3 transporter [27,53,54]. In this context, the present study was undertaken to evaluate the potential of inhibiting the FAS-II enoyl-ACP reductase in *M. abscessus*. In agreement with a previous study [29], our results indicate that the lack of activity of INH in *M. abscessus* presumably relies on the incapacity of $KatG_{MAB}$ to convert INH into an active metabolite, while partial susceptibility levels to INH were recovered when overexpressing the *katG* gene from *M. tuberculosis*. This indicates that while KatG-dependent inhibition of InhA is compromised in *M. abscessus*, it opens, however, the possibility of inhibiting mycolic acid biosynthesis *via* KatG-independent inhibitors of InhA. This proof-of-concept was verified here through the use and characterization of the mode of action of the 4-hydroxy-2-pyridone lead candidate NITD-916, originally identified in a phenotypic screen against *M. tuberculosis* [40].

NITD-916 displayed low MIC values against a wide panel of clinical isolates and exerted an *in vitro* static activity against *M. abscessus* at 1x MIC. This higher MIC value of NITD-916 against *M. abscessus* as compared to *M. tuberculosis* [40] is currently not known but may rely on differences in the cell wall composition and/or architecture of the cell wall between the two species, potentially affecting cell wall permeability to this inhibitor. In addition, *M. abscessus* possesses a large number of efflux pumps, which may also contribute in the lower susceptibility of this species to NITD-916. However, at 1x MIC concentration, the compound did not show any activity in *M. abscessus*-infected macrophages. In contrast, at 10x MIC there was a significant reduction in the intracellular bacterial loads at 1 dpi, which remained comparable at 3 dpi, with similar results obtained against various clinical isolates, with no

distinctions between S and R morphotypes. In general, at 3 dpi, the CFU levels remained equivalent to those in the inoculum (Day 0), indicating that NITD-916 behaves as a bacteriostatic drug in the macrophage under the conditions tested. NITD-916 not only reduced the intracellular bacterial burden but also the proportion of infected macrophages, similarly to RFB, a drug recently proposed to be included in drug regimens to reduce treatment duration of *M. abscessus* pulmonary diseases [55]. Furthermore, exposure of macrophages infected with the R variant to NITD-916 was associated with a reduction in the number and size of cords, presumably resulting from bacterial growth inhibition. Therefore, compounds, such as NITD-916 or RFB, inhibiting intracellular cord formation participate also in the prevention of macrophage death caused by the disruptive activity of cords on macrophage integrity. Consistently, we found that NITD-916 was as active as RFB in CF patient-derived AOs recapitulating the CF airway dysfunctions, such as thick mucus, and with increased susceptibility to *M. abscessus* infection [45]. Thus, our data emphasise an unexploited chemical structure class active against *M. abscessus* infections with promising translational development possibilities for the treatment of CF patients.

From a mechanistic perspective, our genetic and biochemical studies unambiguously indicate that NITD-916 does not undergo bioactivation by KatG prior to binding to $InhA_{MAB}$, but rather inhibits biosynthesis of mycolic acids by directly binding to $InhA_{MAB}$. These assumptions can be inferred from the following results: i) a panel of spontaneous mutants resistant to NITD-916 harboured point mutations in $InhA_{MAB}$ at residue 96 and the mycolic acid pattern of these mutants remained unchanged upon exposure to NITD-916. Replacement of Gly96 by a more bulky residues is associated to NITD-916 resistance, suggesting that conservation of Gly96 is requested for susceptibility to this compound. Multiple sequence alignments of InhA proteins from different mycobacterial species indicate that Gly96 is very well conserved **(Fig. S4)**, thus suggesting that other NTM maybe susceptible to NITD-916 inhibition, although this remains to be investigated in future studies. Interesingly, while replacements occurred only at Gly96 in all *M. abscessus* resistant mutants selected, many more mutations were identified in residues within or near the active site of InhA in *M. tuberculosis* resistant mutants [40,56]. In addition, strains harbouring the $InhA_{MAB}$ G96S or G96V point mutations remained fully sensitive to ETH, as shown previously in *M. tuberculosis* [40]; ii) overexpression of the mutated *inhA* alleles in a susceptible strain conferred resistance to the inhibitor; iii) NITD-916 treatment induced the formation of a KasA-containing complex, reported previously as a marker of InhA inhibition [46]; and iv) NITD-916 could be

identified in a ternary NITD-916:NAD:$InhA_{MAB}$ co-structure. Collectively, these results indicate that NITD-916 shares the same mode of action in *M. abscessus* and *M. tuberculosis* and confirms that the biosynthetic steps of mycolic acids represents an excellent pathway to be further exploited in drug discovey programs against *M. abscessus*. Previous work indicated that NITD-916 has no mutagenic or cardiotoxicity potential and showed no *in vitro* safety pharmacological liabilities and did not inhibit the major CYP450 isoenzyme 3A4 [40], thus stimulating new medicinal chemistry programs for the rational optimization of NITD-916-related analogues targeting $InhA_{MAB}$ with improved efficacy. Changes in the 4-hydroxy 2-pyridone may include substitutions of the R6 lipophilic group and replacement of the R3 phenyl group with other aromatic substituents. In addition, to increase solubility and lipophilicity, phosphate ester prodrugs are typically designed, favoring oral administration and are rapidly hydrolyzed by intestinal alkaline phosphatases. This has been emphasized by synthesizing a 4-hydroxy methyl phosphate ester prodrug of NITD-916, designated NITD-113, displaying improved aqueous solubility by two log orders and with good bioconversion to NITD-916 in mice [40]. The availability of the $InhA_{MAB}$ crystal structure in complex with NAD and NITD-916 will greatly facilitate and guide the chemistry to generate these analogues. In addition, the very high structural conservation between $InhA_{MAB}$ and $InhA_{MTB}$ is a key factor prompting to future testing of a large panel of validated direct $InhA_{MTB}$ inhibitors against *M. abscessus*. Indeed, such direct $InhA_{MTB}$ inhibitory scaffolds have identified in high throughout screenings, encoded library technology or fragment-based screenings and have received considerable attention during these last few years [57]. Another important feature to consider in future studies relies on the possibility to increase the activity of NITD-916 when given in combination with other drugs. Since any *M. abscessus* antibiotic has to be clinically administered in combination with other drugs [22], the absence of drug-drug interactions is critical for clinical development and need to be checked. Using the checkerboard assay, we found that the Frational Inhibitory Concentration Index (FICI) values between NITD-916 and most drugs used in clinics were in the 0.5-1.5 range **(Table S5)**, suggestive of an indifferent interaction between the compounds, thus highlighting the suitability of including NITD-916 in combinational therapy.

CONCLUSIONS

This work reports the potent *in vitro* and intracellular anti-*M. abscessus* activity of NITD-916 and underscores the strong activity of this unexploited chemical scaffold in CF-derived AOs, opening future

possibilities for the treatment of CF patients. Subsequent studies should now advance this compound as well as its derivatives into pre-clinical animal models. Our findings also support the view that targeting mycolic acid biosynthesis has serious translational potential for development into a real tool for treatment and control of *M. abscessus* pulmonary diseases.

METHODS

***Mycobacterium abscessus* strains and culture conditions.** *M. abscessus* subspecies *abscessus* CIP104536^T, *M. abscessus* subspecies *bolletii* CIP108541^T and *M. abscessus* subspecies *massiliense* CIP108297^T reference strains as well as clinical strains from CF and non-CF patients were reported earlier [52,58]. Bacteria were routinely grown and maintained at 37 °C in Middlebrook 7H9 broth (BD Difco) containing 0.025% Tyloxapol (Sigma-Aldrich) and 10% oleic acid, albumin, dextrose, catalase (OADC enrichment; BD Difco) (7H9$^{T/OADC}$) or on Middlebrook 7H10 agar (BD Difco) containing 10% OADC enrichment (7H10^{OADC}). *M. abscessus* carrying pTEC27 and expressing TdTomato was reported earlier and grown in the presence of 1000 µg/mL hygromycin [14]. *M. abscessus* smooth and rough strains were transformed with pSMT3-*katG*$_{MTB}$-*tdTomato* [59] and grown in the presence of 1000 µg/mL hygromycin. For drug susceptibility testing, bacteria were grown in Cation-Adjusted Mueller-Hinton Broth (CaMHB; Sigma-Aldrich). Rifabutin and NITD-916 were purchased from Selleckchem and Merck, respectively, and dissolved in DMSO.

Drug susceptibility testing. The minimal inhibitory concentrations (MIC) were determined according to the CLSI guidelines [60]. The broth micro-dilution method was used in CaMHB with an inoculum of 5x10^6 CFU/mL in exponential growth phase. The bacterial suspension was seeded in 100 µL volumes in all of the wells of a 96-well plate, except for the first column, to which 198 µL of the bacterial suspension was added. In the first column, 2 µL of drug at its highest concentration was added to the first well containing 198 µL of bacterial suspension. Two-fold serial dilutions were then carried out and the plates were incubated for 3-5 days at 30 °C. MICs were recorded by visual inspection. MIC were also determined using Middlebrook 7H9 supplemented with OADC, Sauton's medium or an artificial sputum medium (ASM) containing components of the CF sputum [42].

Growth kinetics. To monitor growth inhibition of *M. abscessus* CIP104536^T (S), 96-well plates were set-up as for MIC determination and serial dilutions of the bacterial suspensions exposed to increasing concentrations of NITD-916 were plated on LB agar plates after 0, 1, 2 and 3 days. Colony-forming units (CFUs) were counted after 4 days of incubation at 37 °C. Results from each drug concentration are representative of 2 independent experiments in triplicates.

Cytotoxicity assay. Human THP-1 monocytes were grown in RPMI medium supplemented with 10% Fetal bovine serum (Sigma Aldrich) (RPMI^{FBS}) and incubated at 37 °C in the presence of 5% CO_2. Cells were differentiated with 20 ng/mL Phorbol Myristate Acetate (PMA) in 96-well flat-bottom tissue culture microplates (2.10^4 cells/well) for 48 hrs at 37 °C with 5% CO_2 and exposed to decreasing concentrations of NITD-916, RFB or INH (starting at 100 µg/mL) for 24 or 72 hrs at 37 °C with 5% CO_2. Following incubation, 10% (vol/vol) resazurin dye was added to each well and left to incubate for another few hours at 37 °C and 5% CO_2. Data was acquired using a fluorescent plate reader (excitation 540 nm, emission 590 nm).

Intracellular killing assay. THP-1 were grown and differentiated into macrophages as reported above but wells were seeded with 10^5 cells. Infection with *M. abscessus* strains was carried out at 37 °C in the presence of 5% CO_2 for 4 hrs at a MOI 2:1. After extensive washing with 1x phosphate buffered saline (PBS), macrophages were incubated with RPMI^{FBS} containing 250 µg/mL amikacin for 2 hrs and washed again with PBS prior to the addition of 500 µL RPMI^{FBS} containing DMSO (negative control) or 500 µL RPMI^{FBS} containing either RFB or NITD-916. Drugs were renewed on a daily basis. Cells were washed with PBS and lysed with 100 µL of 1% Triton X-100 after 1 day or 3 days post-infection. Serial dilutions of macrophage lysates were plated onto LB agar plates and colonies were counted to determine intracellular CFU.

Microscopy-based infectivity assays. Differentiated THP-1 macrophages were grown on coverslips in 24-well plates at a density of 10^5 cells/mL for 48 hrs at 37 °C with 5% CO_2 prior to infection with *M. abscessus* expressing TdTomato for 4 hrs at a MOI of 2:1. After washing and AMK treatment to remove the extracellular bacilli, cells were exposed to DMSO (negative control), RFB or NITD-916 and fixed at 0, 1 and 3 days post-infection with 4% paraformaldehyde (PAF) in 1x PBS for 20 min. Cells were then

permeabilized using 0.2% Triton X-100 for 20 min, blocked with 2% BSA in PBS supplemented with 0.2% Triton X-100 for 20 min, incubated with anti-CD63 antibodies ((Becton Dickinson); dilution 1:1000) for 1 hr and with an Alexa Fluor 488-conjugated anti-mouse secondary antibody ((Molecular Probes, Invitrogen); dilution 1:1000) for 45 min. After 5 min of incubation with DAPI (dilution 1:1000), cells were mounted onto microscope slides using Immu-mount (Calbiochem) and examined with an epifluorescence microscope using a 40X objective. Images were acquired by focusing on combined signals (CD63 in green and *M. abscessus* in red) and captured on a Zeiss Axioimager upright microscope equipped with a 40x and 100x oil objective and processed using ImageJ software. Equal parameters for the capture and scoring of images were consistently applied to all samples. For each condition, approximately 1000 infected macrophages were analyzed. The presence of the intra- or extracellular cords within or among the macrophages infected exclusively with the *M. abscessus* (R) variant were treated in the presence of DMSO, RFB or NITD-916, counted and imaged using full-field upright microscopy. Areas of intracellular cords were quantified using ImageJ.

Selection of resistant *M. abscessus* mutants and target identification. Exponentially growing *M. abscessus* CIP104536^T S and R cultures were plated on LB agar containing 15.6 µg/mL NITD-916, corresponding to 10x MIC. After one week of incubation at 37 °C, four individual colonies deriving from the S and R strains were selected, grown in CaMHB and individually assessed for MIC determination and scored for resistance to NITD-916. Identification of SNPs in the NITD-916-resistant strains was completed by PCR amplification using the primers *MAB_2722c s1 (F)* 5'-GTG GCA GGA CTA CTT GAG GGC-3' and *MAB_2722c s2 (R)* 5'-TCA GAG CAG CTG AGT GTG AGC G -3' to produce a 810 bp amplicon for full coverage sequencing of the *inhA$_{MAB}$* gene.

Cloning and overexpression of the *inhA$_{MAB}$* alleles in *M. abscessus*. Wild-type *inhA$_{MAB}$* and the corresponding mutated genes harbouring the G287T or G286A polymorphisms were amplified by PCR (Q5 polymerase) using genomic DNA prepared from the WT or spontaneous resistant mutants as well the forward 5'-GGG GCA GGA TCC GAG TGG CAG GAC TAC TTG AGG GCA A-3' and reverse 5'-GGG CTA CGA ATT CTG CTA **AGC GTA ATC TGG AAC ATC GTA TGG GTA** GAG CAG CTG AGT GTG AGC GC-3' primers (restriction sites are underlined and HA tag coding sequence is in bold). PCR-amplified fragments were

cloned into the BamHI and EcoRI sites of pMV261 [61] and the resulting plasmids were introduced into *M. abscessus* following selection in the presence of 250 µg/mL kanamycin**.**

Immunoblotting. Bacteria cultures were collected by centrifugation and lysed using 1 mm diameter glass beads and a Mixer Mill MM 301 (Retsch, Germany) at a frequency of 30 Hz for 10 min. Equal amount of total proteins (10 µg) were separated by 12% SDS-PAGE and transferred to a nitrocellulose membrane prior to Western blot analysis. Primary antibodies used were rat anti-HA (1:5000 dilution), rat anti-KasA (1:2000 dilution) or mouse monoclonal antibody 32/15 (1:10 dilution) recognizing the Ag85 complex [62]. After washing, membranes were incubated for 45 min with a anti-rat or anti-mouse antibody conjugated to HRP (dilution 1:5000), incubated with SuperSignal™ West Femto (ThermoFisher Scientific) and revealed using a ChemiDoc MP system (Bio-Rad).

Mycolic acid analysis. To investigate the drug-induced changes in the mycolic acid profile, *M. abscessus* cultures were exposed to increasing drug concentrations of either ethionamide (ETH) included as a positive control or NITD-916 for 1 hr prior to metabolic labeling in the presence of 1 µCi/mL of [2-^{14}C]acetate (59 mCi/mmol, Perkin Elmer) for an additional 2 hrs under shaking at 37 °C. Extraction of total mycolic acids was carried out as previously reported [48]. Briefly, cell pellets were washed and treated with 15% tetrabutylammonium hydroxide (TBAH) at 100 °C overnight. Fatty acids and mycolic acids were methyl-esterified and extracted in diethylether. Lipid extracts were dried and resuspended in dichloromethane and separated by thin-layer chromatography (TLC). Fatty acid methyl esters (FAMEs) and mycolic acid methyl esters (MAMEs) were developed in petroleum ether/acetone (95:5, v/v). The [^{14}C]-labeled FAME and MAME content was analyzed using an Amersham Typhoon imaging system.

Human bronchial organoid culture. The CHU of Toulouse (CHU 19 244 C) and the CNRS (CNRS 205782) approved the use of materials for this study. Organoids were derived from a lung biopsy of a cystic fibrosis heterozygous patient (G542X/1811+1.6kbA→G), as previously reported [45].

Organoid infections. On the infection day, organoids were infected with *M. abscessus* S and R variants adjusted to OD_{600} = 0.2. Organoids in 25 µL drops of Matrigel (Fisher Scientific) were seeded on Nunclon

Delta surface 35x10mm Dish (Thermo Scientific). After Matrigel polymerization, 2 mL of airway organoid complete media [45] without N-Acetylcysteine and without antibiotics were added to each plate. Organoids were microinjected using a Femtojet micro-injector (Eppendorf), as previously described [44]. Two hours after infection, organoids were collected, washed in 1x PBS, embedded into a fresh matrix and treated or not during for 3 days with 1.56 µg/mL or 15.6 µg/mL NITD-916 or 12.5 µg/mL RFB.

Live imaging and colony-forming unit assay. At day 3 post infection, images of the organoids were acquired under an EVOS M7000 Imaging System (20x, at 37 °C with 5% CO_2) (Thermo Scientific). Following image acquisition, infected organoids were individualy collected and lysed in 100 µl of 10% Triton X100 in PBS [44]. Serial dilutions of the lysates were plated on LB agar plates and incubated for 4 days at 37 °C prior to CFU counting.

Crystal structure determination. *M. abscessus* InhA ($InhA_{MAB}$) was expressed and purified using our standard structural genomics expression and purification protocols reported previously [63,64]. Briefly, the *MAB_2722c* gene encoding $InhA_{MAB}$ was cloned from genomic DNA into the bacterial expression vector BG1861, which encodes a non-cleavable N-terminal His_6 tag. The protein was expressed in BL21(DE3) cells with autoinduction media followed by cell lysis and purification *via* nickel affinity then size exclusion chromatography. $InhA_{MAB}$ crystallized at 23.06 mg/mL in the *apo* state in the MCSG1 crystallization screen condition E1 (2 M $(NH_4)_2SO_4$, 0.1 M Hepes pH 7.5); the crystal was cryoprotected with reservoir supplemented with 20% v/v ethylene glycol. $InhA_{MAB}$ crystallized at 23.06 mg/mL with 4 mM NADH in the JCSG+ crystallization screen condition E1 (0.1 M sodium cacodylate pH 6.27, 1.09 M sodium citrate tribasic); the crystal was cryoprotected with reservoir supplemented with 4 mM NADH and 20% v/v ethylene glycol. $InhA_{MAB}$ crystallized at 23.06 mg/mL with 3.5 mM NADH and 3.5 mM NITD-916 in the Index crystallization screen condition H10 (0.2 M sodium citrate tribasic, 20% PEG 3350); the crystal was cryoprotected with reservoir supplemented with 3.5 mM NADH, 3.5 mM NITD-916, and 20% v/v ethylene glycol. The *apo* and the NADH/NITD-916 bound data sets were collected at the Advanced Photon Source beamLine 21 ID-F with a Rayonix MX-300 CCD detector at 0.97872 Å wavelength. The NADH bound data set was collected in house on a Rigaku FR-E+ SuperBright X-ray generator with a Saturn 944+ detector at 1.5406 Å wavelength. The *apo* structure was solved by molecular replacement using MORDA and the *M. tuberculosis* InhA structure (PDB ID 2H7I superceded by 4U0J) as a search

model. The structure was refined with iterative rounds of refinement between Phenix [65] and Coot [66]. X-ray diffraction images have been uploaded to the Integrated Resource for Reproducibility in Macromolecular Crystallography (IRRMC) data base (www.proteindiffraction.org) [67].

Ligand binding via differential scanning fluorimetry (DSF). Sypro dye based DSF experiments were performed on a Bio-Rad CFX-96 thermal cycler at 0.1 mg/mL $InhA_{MAB}$ in a background buffer of 25 mM Tris pH 8.0, 200 mM NaCl, 1 mM TCEP, and 1% v/v glycerol. DMSO was kept contrant at 2% v/v for all measurements. NAD alone or NAD and NITD-916 were added to a final concentration of 1 mM.

Statistical analyses. Statistical analyses were performed on Prism 9.0 (Graphpad) and detailed for each figure legend. *$P \leq 0.05$, ** $P \leq 0.01$, *** $P \leq 0.001$, **** $P \leq 0.0001$.

CONFLICT OF INTEREST

The authors have no conflict of interest to declare.

SUPPORTING INFORMATION

Table S1: MIC of ethionamide and NID-916 against *M. abscessus* in different media.
Table S2. Activity of INH, NITD-916 and the quinoline-INH hybrid **16g** against *M. abscessus* strains overexpressing $KatG_{MTB}$.
Table S3. Crystallographic data collection and refinement statistics.
Table S4. Differential scanning fluorimetry (DSF) measurements on $InhA_{MAB.}$
Table S5. Interactions between NITD-916 and other antibiotics using the checkerboard assay.
Figure S1. Cytotoxicity assay of NITD-916, isoniazid (INH) and rifabutin (RFB) on THP-1 cells.
Figure S2. Percentage of THP-1 macrophages at 0, 1 and 3 days post-infection with *M. abscessus* S in the presence of absence of NITD-916.
Figure S3. Differential scanning fluorimetry (DSF) thermal shift analysis of $InhA_{MAB.}$
Figure S4. Multiple sequence alignments of the InhA proteins.

ACKNOWLEDGMENTS

This study was supported the French National Research Agency ANR-19-CE15-0012-01 (SUNLIVE). We acknowledge the Ministère de l'Enseignement Supérieur, de la Recherche et de l'Innovation for funding the PhD of MA. This work was supported by the National Institutes of Health/National Institute of Alleregy and Infectious Diseases (contract no. HHSN272201700059C) to Peter J. Myler (PI for SSGCID).

CC and SALI were funded by grants from “Vaincre La Mucoviscidose” and “Grégory Lemarchal” foundations (N°RF20210502852/1/1/48). We would like to thank A. Speer for the generous gift of pSMT3-*katG*$_{MTB}$-*tdTomato*.

REFERENCES

(1) Cowman, S.; van Ingen, J.; Griffith, D. E.; Loebinger, M. R. Non-Tuberculous Mycobacterial Pulmonary Disease. *Eur. Respir. J.* **2019**, *54* (1). https://doi.org/10.1183/13993003.00250-2019.

(2) Jönsson, B. E.; Gilljam, M.; Lindblad, A.; Ridell, M.; Wold, A. E.; Welinder-Olsson, C. Molecular Epidemiology of *Mycobacterium abscessus*, with Focus on Cystic Fibrosis. *J. Clin. Microbiol.* **2007**, *45* (5), 1497–1504. https://doi.org/10.1128/JCM.02592-06.

(3) Esther, C. R.; Esserman, D. A.; Gilligan, P.; Kerr, A.; Noone, P. G. Chronic *Mycobacterium abscessus* Infection and Lung Function Decline in Cystic Fibrosis. *J. Cyst. Fibros.* **2010**, *9* (2), 117–123. https://doi.org/10.1016/j.jcf.2009.12.001.

(4) Catherinot, E.; Roux, A.-L.; Macheras, E.; Hubert, D.; Matmar, M.; Dannhoffer, L.; Chinet, T.; Morand, P.; Poyart, C.; Heym, B.; Rottman, M.; Gaillard, J.-L.; Herrmann, J.-L. Acute Respiratory Failure Involving an R Variant of *Mycobacterium abscessus*. *J. Clin. Microbiol.* **2009**, *47* (1), 271–274. https://doi.org/10.1128/JCM.01478-08.

(5) Koh, W.-J.; Jeon, K.; Lee, N. Y.; Kim, B.-J.; Kook, Y.-H.; Lee, S.-H.; Park, Y. K.; Kim, C. K.; Shin, S. J.; Huitt, G. A.; Daley, C. L.; Kwon, O. J. Clinical Significance of Differentiation of *Mycobacterium massiliense* from *Mycobacterium abscessus*. *Am. J. Respir. Crit. Care Med.* **2011**, *183* (3), 405–410. https://doi.org/10.1164/rccm.201003-0395OC.

(6) Adekambi, T.; Sassi, M.; van Ingen, J.; Drancourt, M. Reinstating *Mycobacterium massiliense* and *Mycobacterium bolletii* as Species of the *Mycobacterium abscessus* Complex. *Int. J. Syst. Evol. Microbiol.* **2017**, *67* (8), 2726–2730. https://doi.org/10.1099/ijsem.0.002011.

(7) Johansen, M. D.; Herrmann, J.-L.; Kremer, L. Non-Tuberculous Mycobacteria and the Rise of *Mycobacterium abscessus*. *Nat. Rev. Microbiol.* **2020**, *18* (7), 392–407. https://doi.org/10.1038/s41579-020-0331-1.

(8) Howard, S. T.; Rhoades, E.; Recht, J.; Pang, X.; Alsup, A.; Kolter, R.; Lyons, C. R.; Byrd, T. F. Spontaneous Reversion of *Mycobacterium abscessus* from a Smooth to a Rough Morphotype Is Associated with Reduced Expression of Glycopeptidolipid and Reacquisition of an Invasive Phenotype. *Microbiology (Reading, Engl.)* **2006**, *152* (Pt 6), 1581–1590. https://doi.org/10.1099/mic.0.28625-0.

(9) Gutiérrez, A. V.; Viljoen, A.; Ghigo, E.; Herrmann, J.-L.; Kremer, L. Glycopeptidolipids, a Double-Edged Sword of the *Mycobacterium abscessus* Complex. *Front. Microbiol.* **2018**, *9*, 1145. https://doi.org/10.3389/fmicb.2018.01145.

(10) Roux, A.-L.; Viljoen, A.; Bah, A.; Simeone, R.; Bernut, A.; Laencina, L.; Deramaudt, T.; Rottman, M.; Gaillard, J.-L.; Majlessi, L.; Brosch, R.; Girard-Misguich, F.; Vergne, I.; de Chastellier, C.; Kremer, L.; Herrmann, J.-L. The Distinct Fate of Smooth and Rough *Mycobacterium abscessus* Variants inside Macrophages. *Open Biol.* **2016**, *6* (11). https://doi.org/10.1098/rsob.160185.

(11) Bernut, A.; Viljoen, A.; Dupont, C.; Sapriel, G.; Blaise, M.; Bouchier, C.; Brosch, R.; de Chastellier, C.; Herrmann, J.-L.; Kremer, L. Insights into the Smooth-to-Rough Transitioning in *Mycobacterium*

bolletii Unravels a Functional Tyr Residue Conserved in All Mycobacterial MmpL Family Members. *Mol. Microbiol.* **2016**, *99* (5), 866–883. https://doi.org/10.1111/mmi.13283.

(12) Sánchez-Chardi, A.; Olivares, F.; Byrd, T. F.; Julián, E.; Brambilla, C.; Luquin, M. Demonstration of Cord Formation by Rough *Mycobacterium abscessus* Variants: Implications for the Clinical Microbiology Laboratory. *J. Clin. Microbiol.* **2011**, *49* (6), 2293–2295. https://doi.org/10.1128/JCM.02322-10.

(13) Nessar, R.; Reyrat, J.-M.; Davidson, L. B.; Byrd, T. F. Deletion of the *MmpL4b* Gene in the *Mycobacterium abscessus* Glycopeptidolipid Biosynthetic Pathway Results in Loss of Surface Colonization Capability, but Enhanced Ability to Replicate in Human Macrophages and Stimulate Their Innate Immune Response. *Microbiology (Reading, Engl.)* **2011**, *157* (Pt 4), 1187–1195. https://doi.org/10.1099/mic.0.046557-0.

(14) Bernut, A.; Herrmann, J.-L.; Kissa, K.; Dubremetz, J.-F.; Gaillard, J.-L.; Lutfalla, G.; Kremer, L. *Mycobacterium abscessus* Cording Prevents Phagocytosis and Promotes Abscess Formation. *Proc. Natl. Acad. Sci. U.S.A.* **2014**, *111* (10), E943-952. https://doi.org/10.1073/pnas.1321390111.

(15) Madani, A.; Ridenour, J. N.; Martin, B. P.; Paudel, R. R.; Abdul Basir, A.; Le Moigne, V.; Herrmann, J.-L.; Audebert, S.; Camoin, L.; Kremer, L.; Spilling, C. D.; Canaan, S.; Cavalier, J.-F. Cyclipostins and Cyclophostin Analogues as Multitarget Inhibitors That Impair Growth of *Mycobacterium abscessus*. *ACS Infect. Dis.* **2019**, *5* (9), 1597–1608. https://doi.org/10.1021/acsinfecdis.9b00172.

(16) Lavollay, M.; Dubée, V.; Heym, B.; Herrmann, J.-L.; Gaillard, J.-L.; Gutmann, L.; Arthur, M.; Mainardi, J.-L. *In Vitro* Activity of Cefoxitin and Imipenem against *Mycobacterium abscessus* Complex. *Clin. Microbiol. Infect.* **2014**, *20* (5), O297–O300. https://doi.org/10.1111/1469-0691.12405.

(17) Nessar, R.; Cambau, E.; Reyrat, J. M.; Murray, A.; Gicquel, B. *Mycobacterium abscessus*: A New Antibiotic Nightmare. *J. Antimicrob. Chemother.* **2012**, *67* (4), 810–818. https://doi.org/10.1093/jac/dkr578.

(18) van Ingen, J.; Boeree, M. J.; van Soolingen, D.; Mouton, J. W. Resistance Mechanisms and Drug Susceptibility Testing of Nontuberculous Mycobacteria. *Drug Resist. Updat.* **2012**, *15* (3), 149–161. https://doi.org/10.1016/j.drup.2012.04.001.

(19) Brown-Elliott, B. A.; Nash, K. A.; Wallace, R. J. Antimicrobial Susceptibility Testing, Drug Resistance Mechanisms, and Therapy of Infections with Nontuberculous Mycobacteria. *Clin. Microbiol. Rev.* **2012**, *25* (3), 545–582. https://doi.org/10.1128/CMR.05030-11.

(20) Lopeman, R.; Harrison, J.; Desai, M.; Cox, J. *Mycobacterium abscessus*: Environmental Bacterium Turned Clinical Nightmare. *Microorganisms* **2019**, *7* (3), 90. https://doi.org/10.3390/microorganisms7030090.

(21) Griffith, D. E.; Aksamit, T.; Brown-Elliott, B. A.; Catanzaro, A.; Daley, C.; Gordin, F.; Holland, S. M.; Horsburgh, R.; Huitt, G.; Iademarco, M. F.; Iseman, M.; Olivier, K.; Ruoss, S.; von Reyn, C. F.; Wallace, R. J.; Winthrop, K.; ATS Mycobacterial Diseases Subcommittee; American Thoracic Society; Infectious Disease Society of America. An Official ATS/IDSA Statement: Diagnosis, Treatment, and Prevention of Nontuberculous Mycobacterial Diseases. *Am. J. Respir. Crit. Care Med.* **2007**, *175* (4), 367–416. https://doi.org/10.1164/rccm.200604-571ST.

(22) Floto, R. A.; Olivier, K. N.; Saiman, L.; Daley, C. L.; Herrmann, J.-L.; Nick, J. A.; Noone, P. G.; Bilton, D.; Corris, P.; Gibson, R. L.; Hempstead, S. E.; Koetz, K.; Sabadosa, K. A.; Sermet-Gaudelus, I.; Smyth, A. R.; van Ingen, J.; Wallace, R. J.; Winthrop, K. L.; Marshall, B. C.; Haworth, C. S. US Cystic Fibrosis Foundation and European Cystic Fibrosis Society Consensus Recommendations for the

Management of Non-Tuberculous Mycobacteria in Individuals with Cystic Fibrosis: Executive Summary. *Thorax* **2016**, *71* (1), 88–90. https://doi.org/10.1136/thoraxjnl-2015-207983.

(23) Daley, C. L.; Iaccarino, J. M.; Lange, C.; Cambau, E.; Wallace, R. J.; Andrejak, C.; Böttger, E. C.; Brozek, J.; Griffith, D. E.; Guglielmetti, L.; Huitt, G. A.; Knight, S. L.; Leitman, P.; Marras, T. K.; Olivier, K. N.; Santin, M.; Stout, J. E.; Tortoli, E.; van Ingen, J.; Wagner, D.; Winthrop, K. L. Treatment of Nontuberculous Mycobacterial Pulmonary Disease: An Official ATS/ERS/ESCMID/IDSA Clinical Practice Guideline. *Eur. Respir. J.* **2020**, *56* (1), 2000535. https://doi.org/10.1183/13993003.00535-2020.

(24) Wallace, R. J.; Dukart, G.; Brown-Elliott, B. A.; Griffith, D. E.; Scerpella, E. G.; Marshall, B. Clinical Experience in 52 Patients with Tigecycline-Containing Regimens for Salvage Treatment of *Mycobacterium abscessus* and *Mycobacterium chelonae* Infections. *J. Antimicrob. Chemother.* **2014**, *69* (7), 1945–1953. https://doi.org/10.1093/jac/dku062.

(25) Roux, A.-L.; Catherinot, E.; Soismier, N.; Heym, B.; Bellis, G.; Lemonnier, L.; Chiron, R.; Fauroux, B.; Le Bourgeois, M.; Munck, A.; Pin, I.; Sermet, I.; Gutierrez, C.; Véziris, N.; Jarlier, V.; Cambau, E.; Herrmann, J.-L.; Guillemot, D.; Gaillard, J.-L.; OMA group. Comparing *Mycobacterium massiliense* and *Mycobacterium abscessus* Lung Infections in Cystic Fibrosis Patients. *J. Cyst. Fibros.* **2015**, *14* (1), 63–69. https://doi.org/10.1016/j.jcf.2014.07.004.

(26) Wu, M.-L.; Aziz, D. B.; Dartois, V.; Dick, T. NTM Drug Discovery: Status, Gaps and the Way Forward. *Drug Discov. Today* **2018**, *23* (8), 1502–1519. https://doi.org/10.1016/j.drudis.2018.04.001.

(27) Dupont, C.; Viljoen, A.; Dubar, F.; Blaise, M.; Bernut, A.; Pawlik, A.; Bouchier, C.; Brosch, R.; Guérardel, Y.; Lelièvre, J.; Ballell, L.; Herrmann, J.-L.; Biot, C.; Kremer, L. A New Piperidinol Derivative Targeting Mycolic Acid Transport in *Mycobacterium abscessus*. *Mol. Microbiol.* **2016**, *101* (3), 515–529. https://doi.org/10.1111/mmi.13406.

(28) Luthra, S.; Rominski, A.; Sander, P. The Role of Antibiotic-Target-Modifying and Antibiotic-Modifying Enzymes in *Mycobacterium abscessus* Drug Resistance. *Front. Microbiol.* **2018**, *9*. https://doi.org/10.3389/fmicb.2018.02179.

(29) Gagliardi, A.; Selchow, P.; Luthra, S.; Schäfle, D.; Schulthess, B.; Sander, P. KatG as Counterselection Marker for Nontuberculous Mycobacteria. *Antimicrob. Agents Chemother.* **2020**, *64* (5), e02508-19, /aac/64/5/AAC.02508-19.atom. https://doi.org/10.1128/AAC.02508-19.

(30) Johnsson, K.; Froland, W. A.; Schultz, P. G. Overexpression, Purification, and Characterization of the Catalase-Peroxidase KatG from *Mycobacterium tuberculosis*. *J. Biol. Chem.* **1997**, *272* (5), 2834–2840. https://doi.org/10.1074/jbc.272.5.2834.

(31) Zhang, Y.; Heym, B.; Allen, B.; Young, D.; Cole, S. The Catalase-Peroxidase Gene and Isoniazid Resistance of *Mycobacterium tuberculosis*. *Nature* **1992**, *358* (6387), 591–593. https://doi.org/10.1038/358591a0.

(32) Rozwarski, D. A.; Grant, G. A.; Barton, D. H.; Jacobs, W. R.; Sacchettini, J. C. Modification of the NADH of the Isoniazid Target (InhA) from *Mycobacterium tuberculosis*. *Science* **1998**, *279* (5347), 98–102. https://doi.org/10.1126/science.279.5347.98.

(33) Wilming, M.; Johnsson, K. Spontaneous Formation of the Bioactive Form of the Tuberculosis Drug Isoniazid. *Angew. Chem. Int. Ed. Engl.* **1999**, *38* (17), 2588–2590. https://doi.org/10.1002/(sici)1521-3773(19990903)38:17<2588::aid-anie2588>3.0.co;2-8.

(34) Rawat, R.; Whitty, A.; Tonge, P. J. The Isoniazid-NAD Adduct Is a Slow, Tight-Binding Inhibitor of InhA, the *Mycobacterium tuberculosis* Enoyl Reductase: Adduct Affinity and Drug Resistance.

Proc. Natl. Acad. Sci. U.S.A. **2003**, *100* (24), 13881–13886. https://doi.org/10.1073/pnas.2235848100.

(35) Banerjee, A.; Dubnau, E.; Quemard, A.; Balasubramanian, V.; Um, K. S.; Wilson, T.; Collins, D.; de Lisle, G.; Jacobs, W. R. *InhA*, a Gene Encoding a Target for Isoniazid and Ethionamide in *Mycobacterium tuberculosis*. *Science* **1994**, *263* (5144), 227–230. https://doi.org/10.1126/science.8284673.

(36) Vilchèze, C.; Wang, F.; Arai, M.; Hazbón, M. H.; Colangeli, R.; Kremer, L.; Weisbrod, T. R.; Alland, D.; Sacchettini, J. C.; Jacobs, W. R. Transfer of a Point Mutation in *Mycobacterium tuberculosis inhA* Resolves the Target of Isoniazid. *Nat. Med.* **2006**, *12* (9), 1027–1029. https://doi.org/10.1038/nm1466.

(37) Nguyen, M.; Quémard, A.; Broussy, S.; Bernadou, J.; Meunier, B. Mn(III) Pyrophosphate as an Efficient Tool for Studying the Mode of Action of Isoniazid on the InhA Protein of *Mycobacterium tuberculosis*. *Antimicrob. Agents Chemother.* **2002**, *46* (7), 2137–2144. https://doi.org/10.1128/aac.46.7.2137-2144.2002.

(38) Bhatt, A.; Molle, V.; Besra, G. S.; Jacobs, W. R.; Kremer, L. The *Mycobacterium tuberculosis* FAS-II Condensing Enzymes: Their Role in Mycolic Acid Biosynthesis, Acid-Fastness, Pathogenesis and in Future Drug Development. *Mol. Microbiol.* **2007**, *64* (6), 1442–1454. https://doi.org/10.1111/j.1365-2958.2007.05761.x.

(39) Vilchèze, C.; Morbidoni, H. R.; Weisbrod, T. R.; Iwamoto, H.; Kuo, M.; Sacchettini, J. C.; Jacobs, W. R. Inactivation of the *inhA*-Encoded Fatty Acid Synthase II (FASII) Enoyl-Acyl Carrier Protein Reductase Induces *Accumulation* of the FASI End Products and Cell Lysis of *Mycobacterium smegmatis*. *J. Bacteriol.* **2000**, *182* (14), 4059–4067. https://doi.org/10.1128/jb.182.14.4059-4067.2000.

(40) Manjunatha, U. H.; S. Rao, S. P.; Kondreddi, R. R.; Noble, C. G.; Camacho, L. R.; Tan, B. H.; Ng, S. H.; Ng, P. S.; Ma, N. L.; Lakshminarayana, S. B.; Herve, M.; Barnes, S. W.; Yu, W.; Kuhen, K.; Blasco, F.; Beer, D.; Walker, J. R.; Tonge, P. J.; Glynne, R.; Smith, P. W.; Diagana, T. T. Direct Inhibitors of InhA Are Active against *Mycobacterium tuberculosis*. *Sci. Transl. Med.* **2015**, *7* (269), 269ra3-269ra3. https://doi.org/10.1126/scitranslmed.3010597.

(41) Johansen, M. D.; Daher, W.; Roquet-Banères, F.; Raynaud, C.; Alcaraz, M.; Maurer, F. P.; Kremer, L. Rifabutin Is Bactericidal against Intracellular and Extracellular Forms of *Mycobacterium abscessus*. *Antimicrob. Agents Chemother.* **2020**, *64* (11), e00363-20, /aac/64/11/AAC.00363-20.atom. https://doi.org/10.1128/AAC.00363-20.

(42) Kirchner, S.; Fothergill, J. L.; Wright, E. A.; James, C. E.; Mowat, E.; Winstanley, C. Use of Artificial Sputum Medium to Test Antibiotic Efficacy Against *Pseudomonas aeruginosa* in Conditions More Relevant to the Cystic Fibrosis Lung. *J. Vis. Exp.* **2012**, No. 64, 3857. https://doi.org/10.3791/3857.

(43) Lefebvre, A.-L.; Dubée, V.; Cortes, M.; Dorchêne, D.; Arthur, M.; Mainardi, J.-L. Bactericidal and Intracellular Activity of β-Lactams against *Mycobacterium abscessus*. *J. Antimicrob. Chemother.* **2016**, *71* (6), 1556–1563. https://doi.org/10.1093/jac/dkw022.

(44) Iakobachvili, N.; Leon-Icaza, S. A.; Knoops, K.; Sachs, N.; Mazères, S.; Simeone, R.; Peixoto, A.; Bernard, C.; Murris-Espin, M.; Mazières, J.; Cam, K.; Chalut, C.; Guilhot, C.; López-Iglesias, C.; Ravelli, R. B. G.; Neyrolles, O.; Meunier, E.; Lugo-Villarino, G.; Clevers, H.; Cougoule, C.; Peters, P. J. Mycobacteria-Host Interactions in Human Bronchiolar Airway Organoids. *Mol. Microbiol.* **2022**, *117* (3), 682–692. https://doi.org/10.1111/mmi.14824.

(45) Leon-Icaza, S. A.; Bagayoko, S.; Iakobachvili, N.; Ferrand, C.; Aydogan, T.; Bernard, C.; Dafun, A. S.; Murris-Espin, M.; Mazières, J.; Bordignon, P. J.; Mazères, S.; Bernes-Lasserre, P.; Ramé, V.; Lagarde, J.-M.; Marcoux, J.; Bousquet, M. P.; Chalut, C.; Guilhot, C.; Clevers, H.; Peters, P. J.; Molle, V.; Lugo-Villarino, G.; Cam, K.; Berry, L.; Meunier, E.; Cougoule, C. Cystic Fibrosis Patient-Derived Bronchial Organoids Unveil Druggable Pathways against *Mycobacterium abscessus* Infection; preprint; Cell Biology, 2022. https://doi.org/10.1101/2022.01.03.474765.

(46) Kremer, L.; Dover, L. G.; Morbidoni, H. R.; Vilchèze, C.; Maughan, W. N.; Baulard, A.; Tu, S.-C.; Honoré, N.; Deretic, V.; Sacchettini, J. C.; Locht, C.; Jacobs, W. R.; Besra, G. S. Inhibition of InhA Activity, but Not KasA Activity, Induces Formation of a KasA-Containing Complex in Mycobacteria. *J. Biol. Chem.* **2003**, *278* (23), 20547–20554. https://doi.org/10.1074/jbc.M302435200.

(47) Halloum, I.; Carrère-Kremer, S.; Blaise, M.; Viljoen, A.; Bernut, A.; Le Moigne, V.; Vilchèze, C.; Guérardel, Y.; Lutfalla, G.; Herrmann, J.-L.; Jacobs, W. R.; Kremer, L. Deletion of a Dehydratase Important for Intracellular Growth and Cording Renders Rough *Mycobacterium abscessus* Avirulent. *Proc. Natl. Acad. Sci. U.S.A.* **2016**, *113* (29), E4228-4237. https://doi.org/10.1073/pnas.1605477113.

(48) Dover, L. G.; Alahari, A.; Gratraud, P.; Gomes, J. M.; Bhowruth, V.; Reynolds, R. C.; Besra, G. S.; Kremer, L. EthA, a Common Activator of Thiocarbamide-Containing Drugs Acting on Different Mycobacterial Targets. *Antimicrob. Agents Chemother.* **2007**, *51* (3), 1055–1063. https://doi.org/10.1128/AAC.01063-06.

(49) Rozwarski, D. A.; Vilchèze, C.; Sugantino, M.; Bittman, R.; Sacchettini, J. C. Crystal Structure of the *Mycobacterium tuberculosis* Enoyl-ACP Reductase, InhA, in Complex with NAD^+ and a C16 Fatty Acyl Substrate. *J. Biol. Chem.* **1999**, *274* (22), 15582–15589. https://doi.org/10.1074/jbc.274.22.15582.

(50) Kuo, M. R.; Morbidoni, H. R.; Alland, D.; Sneddon, S. F.; Gourlie, B. B.; Staveski, M. M.; Leonard, M.; Gregory, J. S.; Janjigian, A. D.; Yee, C.; Musser, J. M.; Kreiswirth, B.; Iwamoto, H.; Perozzo, R.; Jacobs, W. R.; Sacchettini, J. C.; Fidock, D. A. Targeting Tuberculosis and Malaria through Inhibition of Enoyl Reductase: Compound Activity and Structural Data. *J. Biol. Chem.* **2003**, *278* (23), 20851–20859. https://doi.org/10.1074/jbc.M211968200.

(51) Grzegorzewicz, A. E.; Eynard, N.; Quémard, A.; North, E. J.; Margolis, A.; Lindenberger, J. J.; Jones, V.; Korduláková, J.; Brennan, P. J.; Lee, R. E.; Ronning, D. R.; McNeil, M. R.; Jackson, M. Covalent Modification of the *Mycobacterium tuberculosis* FAS-II Dehydratase by Isoxyl and Thiacetazone. *ACS Infect. Dis.* **2015**, *1* (2), 91–97. https://doi.org/10.1021/id500032q.

(52) Halloum, I.; Viljoen, A.; Khanna, V.; Craig, D.; Bouchier, C.; Brosch, R.; Coxon, G.; Kremer, L. Resistance to Thiacetazone Derivatives Active against *Mycobacterium abscessus* Involves Mutations in the MmpL5 Transcriptional Repressor MAB_4384. *Antimicrob. Agents Chemother.* **2017**, *61* (4), e02509-16. https://doi.org/10.1128/AAC.02509-16.

(53) Kozikowski, A. P.; Onajole, O. K.; Stec, J.; Dupont, C.; Viljoen, A.; Richard, M.; Chaira, T.; Lun, S.; Bishai, W.; Raj, V. S.; Ordway, D.; Kremer, L. Targeting Mycolic Acid Transport by Indole-2-Carboxamides for the Treatment of *Mycobacterium abscessus Infections*. *J. Med. Chem.* **2017**, *60* (13), 5876–5888. https://doi.org/10.1021/acs.jmedchem.7b00582.

(54) Raynaud, C.; Daher, W.; Johansen, M. D.; Roquet-Banères, F.; Blaise, M.; Onajole, O. K.; Kozikowski, A. P.; Herrmann, J.-L.; Dziadek, J.; Gobis, K.; Kremer, L. Active Benzimidazole Derivatives Targeting the MmpL3 Transporter in *Mycobacterium abscessus*. *ACS Infect. Dis.* **2020**, *6* (2), 324–337. https://doi.org/10.1021/acsinfecdis.9b00389.

(55) Dick, T. Rifabutin: A Repurposing Candidate for *Mycobacterium abscessus* Lung Disease. *Front. Microbiol.* **2020**, *11*, 371. https://doi.org/10.3389/fmicb.2020.00371.
(56) McNeil, M. B.; Dennison, D.; Shelton, C.; Flint, L.; Korkegian, A.; Parish, T. Mechanisms of Resistance against NITD-916, a Direct Inhibitor of *Mycobacterium tuberculosis* InhA. *Tuberculosis (Edinb)* **2017**, *107*, 133–136. https://doi.org/10.1016/j.tube.2017.09.003.
(57) Prasad, M. S.; Bhole, R. P.; Khedekar, P. B.; Chikhale, R. V. *Mycobacterium* Enoyl Acyl Carrier Protein Reductase (InhA): A Key Target for Antitubercular Drug Discovery. *Bioorg. Chem.* **2021**, *115*, 105242. https://doi.org/10.1016/j.bioorg.2021.105242.
(58) Singh, S.; Bouzinbi, N.; Chaturvedi, V.; Godreuil, S.; Kremer, L. *In Vitro* Evaluation of a New Drug Combination against Clinical Isolates Belonging to the *Mycobacterium abscessus* Complex. *Clin. Microbiol. Infect.* **2014**, *20* (12), O1124-1127. https://doi.org/10.1111/1469-0691.12780.
(59) Ho, V. Q. T.; Verboom, T.; Rong, M. K.; Habjan, E.; Bitter, W.; Speer, A. Heterologous Expression of EthA and KatG in *Mycobacterium marinum* Enables the Rapid Identification of New Prodrugs Active against *Mycobacterium tuberculosis*. *Antimicrob. Agents Chemother.* **2021**, *65* (4), e01445-20. https://doi.org/10.1128/AAC.01445-20.
(60) Woods, GL; Brown-Elliott, BA; Conville, PS; Desmond, EP; Hall, GS; Lin G; Pfyffer GE; Ridderhof, JC; Siddiqi, SH; Wallace, RJ. *Susceptibility Testing of Mycobacteria, Nocardiae and Other Aerobic Actinomycetes: Approved Standard*, Second Edition (M24-A2). Clinical and Laboratory Standards Institute: Wayne, PA 2011.; 2011.
(61) Stover, C. K.; de la Cruz, V. F.; Fuerst, T. R.; Burlein, J. E.; Benson, L. A.; Bennett, L. T.; Bansal, G. P.; Young, J. F.; Lee, M. H.; Hatfull, G. F. New Use of BCG for Recombinant Vaccines. *Nature* **1991**, *351* (6326), 456–460. https://doi.org/10.1038/351456a0.
(62) Viljoen, A.; Richard, M.; Nguyen, P. C.; Fourquet, P.; Camoin, L.; Paudal, R. R.; Gnawali, G. R.; Spilling, C. D.; Cavalier, J.-F.; Canaan, S.; Blaise, M.; Kremer, L. Cyclipostins and Cyclophostin Analogs Inhibit the Antigen 85C from *Mycobacterium tuberculosis* Both *in Vitro* and *in Vivo*. *J. Biol. Chem.* **2018**, *293* (8), 2755–2769. https://doi.org/10.1074/jbc.RA117.000760.
(63) Bryan, C. M.; Bhandari, J.; Napuli, A. J.; Leibly, D. J.; Choi, R.; Kelley, A.; Van Voorhis, W. C.; Edwards, T. E.; Stewart, L. J. High-Throughput Protein Production and Purification at the Seattle Structural Genomics Center for Infectious Disease. *Acta Crystallogr. Sect. F Struct. Biol. Cryst. Commun.* **2011**, *67* (Pt 9), 1010–1014. https://doi.org/10.1107/S1744309111018367.
(64) Choi, R.; Kelley, A.; Leibly, D.; Hewitt, S. N.; Napuli, A.; Van Voorhis, W. Immobilized Metal-Affinity Chromatography Protein-Recovery Screening Is Predictive of Crystallographic Structure Success. *Acta Crystallogr. Sect. F Struct. Biol. Cryst. Commun.* **2011**, *67* (Pt 9), 998–1005. https://doi.org/10.1107/S1744309111017374.
(65) Adams, P. D.; Afonine, P. V.; Bunkóczi, G.; Chen, V. B.; Davis, I. W.; Echols, N.; Headd, J. J.; Hung, L.-W.; Kapral, G. J.; Grosse-Kunstleve, R. W.; McCoy, A. J.; Moriarty, N. W.; Oeffner, R.; Read, R. J.; Richardson, D. C.; Richardson, J. S.; Terwilliger, T. C.; Zwart, P. H. PHENIX: A Comprehensive Python-Based System for Macromolecular Structure Solution. *Acta Crystallogr. D Biol. Crystallogr.* **2010**, *66* (Pt 2), 213–221. https://doi.org/10.1107/S0907444909052925.
(66) Emsley, P.; Cowtan, K. Coot: Model-Building Tools for Molecular Graphics. *Acta Crystallogr. D. Biol. Crystallogr.* **2004**, *60* (Pt 12 Pt 1), 2126–2132. https://doi.org/10.1107/S0907444904019158.

(67) Grabowski, M.; Cymborowski, M.; Porebski, P. J.; Osinski, T.; Shabalin, I. G.; Cooper, D. R.; Minor, W. The Integrated Resource for Reproducibility in Macromolecular Crystallography: Experiences of the First Four Years. *Struct. Dyn.* **2019**, *6* (6), 064301. https://doi.org/10.1063/1.5128672.